Poly-Target Selection Identifies RNA Broad-Spectrum Inhibitors of HIV Reverse Transcriptases

Khalid K. Alam[1,2,5], Jonathan L. Chang[2,3], Margaret J. Lange[2,3], Phuong D.M. Nguyen[1,2], Andrew W. Sawyer[1,2], & Donald H. Burke[1,2,3,4,*]

[1]Department of Biochemistry, [2]Bond Life Sciences Center, [3]Department of Molecular Microbiology and Immunology, [4]Department of Biological Engineering, University of Missouri, Columbia, MO, USA

[5]Current address: Department of Chemical and Biological Engineering, Northwestern University, Evanston, IL, USA

*Corresponding author: burkedh@missouri.edu

Reverse transcriptase (RT) inhibitors are core components of antiretroviral therapies; however, HIV's high mutation rate prompts the emergence of drug resistance and necessitates new inhibitors with high genetic barriers to resistance. RNA aptamers that have been selected to bind RT exhibit potent RT inhibition and suppress viral replication when targeting the strain-specific RT that they were originally selected to bind, but some of these same, otherwise potent aptamers fail against both single-point mutant and phylogenetically-diverse RTs. We hypothesized that a subset of the total aptamer population in libraries pre-enriched against a single RT may exhibit broad-spectrum RT binding and inhibition, and we devised a multiplexed Poly-Target selection approach to elicit those phenotypes against a panel of diverse lentiviral RTs. High-throughput sequencing of starting, negative, and final libraries, followed by coenrichment analysis of parallel and duplicate selection trajectories, narrowed the list of candidate aptamers by orders of magnitude. Biochemical characterization of candidates identified a novel aptamer motif and several rare and unobserved variants of previously-known motifs that inhibited recombinant RTs from HIV-1, HIV-2 and SIV to varying degrees. These broad-spectrum aptamers also suppressed replication of viruses carrying phylogenetically-diverse RTs. The Poly-Target selection and coenrichment approach described herein is a generalizable strategy for identifying broad-spectrum behavior and cross-reactivity among related targets from combinatorial libraries.

INTRODUCTION

Human immunodeficiency virus type 1 (HIV-1), the predominant etiologic agent of acquired immunodeficiency syndrome (AIDS), remains a major global health concern. While control of viral replication through appropriate surveillance and highly active antiretroviral therapy (HAART) has dramatically improved patient outcomes, several challenges remain in the absence of a universal functional cure or vaccine. The high rate of viral replication, coupled with the low fidelity of reverse transcriptase (RT) (1) and recombination between genetically diverse strains (2), result in a high mutation rate for the virus (3). In addition, selection pressures exerted by antiviral compounds in patients have led to the emergence of drug resistant strains of HIV (4), requiring continued development of therapeutics that provide a high genetic barrier to resistance. Because reverse transcription of the viral RNA genome into DNA is an early and essential step in the viral life cycle with a non-analogous function in hosts, inhibition of RT remains a core component in HIV treatment. RT's major functions are to copy the viral RNA genome into DNA (polymerase activity) and to degrade the viral RNA after cDNA synthesis (RNase activity) (5). Current guidelines for HAART recommend a three-drug regimen consisting of two nucleoside reverse transcriptase inhibitors in combination with an agent from the non-nucleoside RT inhibitor, integrase inhibitor, or protease inhibitor classes (6). Concerns with toxicity, patient adherence, and the continual emergence of drug resistance against RT and other HIV inhibitors motivate efforts to identify alternative therapeutic strategies for the treatment of infection and eradication of the viral reservoir (7).

Aptamers are single-stranded nucleic acids that bind with high affinity to defined molecular targets, and they can be generated through an iterative *in vitro* selection process known as SELEX (8-10). RNA aptamers selected against HIV-1 RT are able to bind RT and inhibit its enzymatic activities, and they overwhelmingly form pseudoknot structures (11-13). These pseudoknot RNA aptamers show robust *in vitro* inhibition of the RT they were selected to bind (14) and they suppress viral replication and infectivity in cell culture (15-19). Structural and biophysical investigations suggest that these pseudoknot RNA aptamers bind the closed conformation of RT in a positively-charged groove, 50-60 Å in length, that spans the polymerase and RNase H domains (20, 21). This same groove can accommodate 16-19 base pairs of nucleic acid and naturally binds a duplex of viral RNA and host $tRNA_{Lys}$ primer. An observation from our lab is that a common polymorphism in this groove, near the polymerase active site (K277 in the p66 subunit), confers resistance to the Family 1 Pseudoknot subset of RNA aptamers (22), thereby preventing broad-spectrum inhibition. In contrast, single stranded DNA aptamers selected against RT (23) demonstrate broad-spectrum inhibition *in vitro* (24-27), but their use in genetic therapy is complicated by the requirement to produce or deliver single stranded DNA in the relevant cells.

High-throughput sequencing of anti-RT RNA aptamer libraries recently revealed several additional motifs capable of RT binding and inhibition, including the (6/5) asymmetric loop (28) and the UCAA bulge (29). These non-pseudoknot motifs were difficult to detect with low-throughput sequencing, as their low sampling frequencies were eclipsed by the abundance of aptamers that carried pseudoknot motifs (>93% in one library (28)). Although these novel motifs were neither selected nor initially characterized for their broad-spectrum inhibition, recent work, done in conjunction with the work described here, demonstrated that these non-pseudoknot motifs were capable of broad-spectrum suppression of viral replication when actively encapsidated into nascent virions (19). The additional functional diversity present in these libraries suggested that new genotypes and phenotypes were potentially accessible under different selection conditions.

Herein we describe a Poly-Target selection method developed to enrich for RNA aptamers with broad-spectrum binding and inhibition of diverse primate lentiviral RTs. Rather than performing a *de novo* selection from a random-sequence library, we utilized two well-characterized libraries that had been pre-enriched for binding to RT from a specific HIV-1 strain. Negative selections against nitrocellulose

were performed to remove RT-independent binders, followed by three rounds of positive selections against a panel of seven diverse lentiviral RTs, in parallel. Each selection trajectory was performed in duplicate, and high-throughput sequencing of the starting, negative, and final libraries enabled an informatics approach to identify candidate aptamers through coenrichment analysis of the various selection trajectories. Motif analysis and biochemical screening of candidates identified several rare variants of known motifs and one previously unknown motif capable of varying degrees of broad-spectrum inhibition of RT polymerase activity. Furthermore, these broad-spectrum aptamers inhibit RTs that were not included in the selection panel and suppress viral replication of constructs containing diverse RTs.

RESULTS

Poly-Target Selection Panel

Two distinct, pre-enriched aptamer libraries with randomized regions of either 70 or 80 nucleotides (70N and 80N, respectively) were used to initiate Poly-Target selection. These libraries were originally selected *in vitro* against recombinant RT from a group M, subtype B strain of HIV-1 (BH10) (13). In these original selections, partitioning for protein-bound RNA was accomplished through eleven rounds of nitrocellulose filtration and three rounds of native gel shifts, for a total of fourteen rounds. The vast majority of RNA aptamers identified through low-throughput Sanger sequencing of these populations were those that form pseudoknot structures, which bind with low nanomolar affinity and inhibit the RT by competing with primer-template for access to the enzyme. High-throughput sequencing recently enabled deeper analyses of these libraries and revealed previously undetected motifs, such as the 6/5 asymmetric loop ((6/5)AL) (28) and UCAA bulge (29), suggesting that significant diversity exists within these libraries. A central goal of the present work is to exploit untapped diversity within these pre-enriched libraries by identifying low-abundance structural motifs that may offer broad-spectrum binding and inhibition of RTs.

To elicit broad-spectrum phenotypes from the pre-enriched libraries, we assembled a panel of phylogenetically diverse primate lentiviral RTs (22) (**Supplementary Figure 1**). The panel of targets included RTs from multiple strains of the major group (group M) of HIV-1. Group M is responsible for the global pandemic and is further divided into subtypes and circulating recombinant forms (CRFs) that contain genomic segments from two or more subtypes and represent a growing percentage of worldwide infections. Group M, subtype B (M:B) HIV-1 is the most prevalent form across the Americas, Western Europe and Australia, and accounts for 11% of global HIV infections (30). HXB2 is an M:B strain closely related to the original selection target (98.9% by amino acid identity), and it is often used as a reference strain for sequence comparisons. We therefore included RT from strain HXB2 in the panel as a “continuity control.” Also included was an R277K single point mutant of HXB2, a natural polymorphism which confers resistance to inhibition by Family 1 Pseudoknot aptamers *in vitro* (22) and in cell culture (19), to enrich for aptamers that bind in spite of this escape mutation (henceforth referred to as R277K). However, most HIV-1 infections worldwide are from non-B subtypes of Group M. Therefore, RT from strain 94CY was included as a representative of subtype A (M:A) HIV-1, which is responsible for approximately 12% of global infections and is common throughout Eastern Europe, Eastern Africa and Central Asia (30). We also included RT from 93TH, which groups phylogenetically within CRF01_AE, a circulating recombinant form that is the predominant form of HIV in Southeast Asia (30) and carries genomic segments corresponding to subtypes A and E.

The selection panel also included RTs from several non-group M strains of HIV-1 and simian immunodeficiency virus (SIV_{cpz}*Pts*). Although these additional strains are of less epidemiological relevance, they help to capture the broader genetic diversity of lentiviruses (**Supplementary Figure 1**). The outlier group of HIV-1 (group O) is estimated to infect 1-5% of HIV-1 patients, mainly in West and Central Africa (31). Group O is phylogenetically distinct from group M and originated independently. We therefore included an RT from the group O strain MVP. Because HIV-1 arose from zoonotic

transmission of SIV_{cpz} from chimpanzees (32), we included an RT from the TAN1B strain of SIV_{cpz}. Finally, we included RT from the EHO strain of HIV-2, which is only distantly related to HIV-1, to further broaden the scope of the Poly-Target selection. Selecting independently against each of these RTs presents a gradient of selection pressures on the pre-enriched library to search the sequence space for ligands that are capable of making molecular contacts with conserved features of primate lentiviral RTs. A table depicting the unabbreviated name of the strains, their reference sequences, and changes in their amino acid sequence relative to the database reference sequences are provided in **Supplementary Table S1**.

Poly-Target Selection, High-throughput Sequencing and Bioinformatics

A schematic for the Poly-Target selection strategy is shown in **Figure 1**. Pre-enriched round 14 libraries were transcribed and partially depleted for nitrocellulose-binding species. Libraries were then separated into replication populations (A and B) and further split into independent populations for each of the seven RT targets. For each round of Poly-Target selections, transcribed RNA for a given trajectory was independently incubated with a single RT from the selection panel. Bound RNA:RT complexes were captured on nitrocellulose filters, and the recovered RNA was reverse transcribed into cDNA and then PCR amplified for additional rounds of selection or for high-throughput sequencing (HTS). Each selection trajectory was performed for a total of three rounds, after which the starting round 14 libraries, the nitrocellulose binding populations, and the round 17 libraries were submitted for HTS.

HTS of the libraries generated over 184 million raw reads. Demultiplexing, trimming and quality filtering (**Supplementary Figure S2**) of sequences left over 52 million high quality reads for the 70N library and 54 million for the 80N library. Each selection trajectory contained an average of three million total reads and 35,000 to >100,000 unique sequences (**Supplementary Table S2**). The average number of reads per unique sequence increased for all populations, indicating enrichment and convergence on sequence space within each library, with the exception of 70N TAN1B (A), which was the only population with fewer than one million total reads (**Supplementary Figure S3**). Aptamer populations were further processed by the FASTAptamer toolkit to determine sequence frequencies, compare populations and calculate enrichment of each unique sequence relative to the starting round 14 library (33). Sequences were clustered with FASTAptamer using Levenshtein edit distance – a string similarity metric that calculates the minimum number of insertions, deletions and substitutions necessary to transform one sequence into another. Sequences within a small edit distance from each other likely diverged from a parent sequence in an earlier population and grouping them into a single cluster simplifies analysis. Based on previous observations that sequences in these populations typically diverge by less than 10% from their parent sequences (28), we defined clusters as having a maximum edit distance of 7 for the 70N library and 8 for the 80N library.

To determine the degree to which replicate selections against the same target experienced similar evolutionary paths, normalized sequence frequencies from the A and B trajectories for each target were compared using FASTAptamer-Compare (33). For both the 70N and 80N round 14 libraries, we observe a tight $y = x$ relationship between replicates (**Supplementary Figures S4A and S5A**), suggesting highly similar input diversity for each pair of replicate trajectories for a given target. In contrast, comparing sequence frequencies between replicate trajectories after three rounds show a multimodal distribution for many populations, wherein different subsets of sequences either enrich, remain neutral, or deplete (**Supplementary Figures S4B-H and S5B-H**). These minor variations between replicate trajectories likely reflect stochastic variations in sample handling (34) and highlight the potential value in providing multiple, independent evolutionary opportunities for a given sequence to enrich or deplete. As expected, distributions were widened more dramatically when comparing different selection rounds or selections against different targets (**Supplementary Figures S6 and S7**).

Coenrichment Analysis Identifies Candidate Broad-Spectrum Aptamers

Sequences from the Poly-Target selection that enriched in more than one selection trajectory were expected to be the most promising candidates as broad-spectrum aptamers. As a first step towards coenrichment analysis, we identified sequences within each post-selection population that met a given enrichment threshold, which we defined as a two-fold or greater increase in reads per million (RPM) relative to the starting round 14 population (**Supplementary Figure S8A**). To mitigate the potential impact of low abundance sampling artifacts, we confined this analysis to sequences with an aggregate RPM ≥ 10 when summed across the populations being compared (e.g., round 14 RPM + round 17 RPM). We also included sequences that were below the detection limit in round 14 libraries but later increased in relative abundance and were sampled with ≥ 10 RPM in round 17, although their absence in round 14 precluded calculating an enrichment ratio. On average, each trajectory had approximately 1,800 sequences that met our enrichment criteria (**Supplementary Table S3**). Depleting sequences were similarly flagged by identifying sequences with aggregate RPMs of ≥ 10 that either decreased by at least two-fold (0.5-fold enrichment) in each trajectory, or that were present in round 14 at ≥ 10 RPM and below the detection limit in round 17. Each trajectory had approximately 2,600 sequences that met our depletion criteria (**Supplementary Table S3**). In nearly all trajectories, the number of sequences that depleted throughout the course of the selections exceeded the number that enriched.

We next identified the sets of sequences that experienced coenrichment or codepletion in two or more trajectories (**Supplementary Figure S8B**). These were pooled according to starting library and replicate, irrespective of which individual trajectories provided the basis for identifying them as coenriching or codepleting. Each starting library (70N and 80N) and each replicate within them (A and B) were analyzed independently, thereby generating four unique sets of coenriched sequences (average of 3,200 per set) and four sets of codepleted sequences (average of 3,500 per set) (**Supplementary Table S4**). Sequences demonstrating coenrichment or codepletion in the negative nitrocellulose selections were eliminated from analysis, reducing each library replicate to an average of 2,500 coenriched and 1,800 codepleted sequences. Dataset complexity was further reduced by reclustering each set of coenriched or codepleted sequences into sequence families. To facilitate comparison across trajectories, the identified sequences were mapped to their cluster identity from round 14 (**Supplementary Figure S9**). Clustering and mapping in this manner allowed us to readily discern highly-enriched clusters that arose in either or both replicate trajectories.

As individual clusters can contain numerous sequence variants, individual sequences within those clusters can sample advantageous or deleterious mutations. To focus on clusters where the majority of sequences exhibited coenrichment with minimal codepletion, we coupled the output from the coenrichment and codepletion analysis (**Supplementary Figure S10**). Fourteen clusters from the 70N libraries and nineteen clusters from the 80N libraries were chosen for further characterization based on this analysis (33 total). Two clusters that heavily depleted in the 70N trajectory (70N 2 and 70N 3) were also included to test whether codepletion is predictive of low fitness. For each cluster, the most abundant corresponding sequence in round 14 was chosen to represent the entire cluster in biochemical characterization. Candidate aptamers are named by their library of origin and their cluster identity in the pre-enriched round 14 libraries (*e.g.* aptamer 70N 89 is the 89th most abundant sequence in the 70N round 14 library and served as the seed sequence for the 89th cluster). Sequences that were not sampled in the round 14 libraries were named according to the cluster identity generated in the coenrichment analysis. A heat map of genotypic frequencies for each selected candidate aptamer in each trajectory is shown in **Figure 2A**, with more detailed information on the frequency of individual sequences in each trajectory detailed in **Supplementary Table S5**.

Genotype Analysis Identifies Known, Rare and Previously Unobserved Sequence Motifs

The 33 sequences identified above (**Figure 2, Supplementary Figure S9**, **Supplementary Table S5**) and two additional sequences that both heavily codepleted were analyzed for the presence of sequence motifs that have been previously shown to robustly inhibit subtype B RTs *in vitro* and suppress viral

replication in cell culture (15-19, 28, 29). The FASTAptamer-Search function of the FASTAptamer toolkit (33) was employed to search for degenerate sequence motifs, and Mfold (35) was used to generate secondary structure predictions. Although Mfold is unable to predict pseudoknot motifs, we reasoned that it would help to provide structural evidence for UCAA and (6/5)AL motifs and could help identify aptamers with novel motifs. Applying this approach with relaxed search constraints identified the three major secondary structural motifs known to bind HIV-1 RT – pseudoknot, (6/5)AL and UCAA – within most, but not all of these 35 sequences.

FASTAptamer-Search identified ten sequences as Family 1 Pseudoknot (**Supplementary Table S6**), including the two 70N sequences noted above as having codepleted significantly (70N 2 and 70N 3). The Family 1 Pseudoknot motif (F1Pk) is characterized by the string UCCG-$N_{7/8}$-CGGGANAA$N_{\geq 3}$, where N refers to any nucleotide, and $N_{\geq 3}$ refers to a segment that base pairs with at least three connector nucleotides to form Stem II (**Figure 2B**) (11-13, 28). Some of these F1Pk-like aptamers diverged slightly from the expected sequence motif definition, and their enrichment patterns appear to reflect their specialized characteristics. For example, 70N 27 and 70N 73 contained only two potential base pairs in Stem II. They also showed the strongest enrichment in the EHO (HIV-2) trajectory, potentially allowing for this variation of the F1Pk motif to maximize contacts with that particular RT. Similarly, while nine of the ten F1Pk sequences contain a seven or eight nucleotide connector, 70N 144 contains a ten-nucleotide connector. The strong enrichment of this sequence in all of the trajectories, including the nitrocellulose binding population, indicates that it may be a selection parasite, rather than a high-affinity RT binder.

The UCAA motif is minimally defined by a four-nucleotide UCAA bulge flanked by AC/GU closing base pairs on one end and by a stem that is interrupted by a single unpaired U on the other end (**Figure 2D**) (29). Searching for the UCAA motif identified four sequences, two of which (80N 16 and 80N 148) conformed fully to the motif definition. 80N 16 is identical to aptamer 80.103, which had been identified previously and shown to inhibit HXB2 RT *in vitro* and to suppress viral replication in cell culture (29). The core element within 80N 148 was validated through aptamer truncation and RT inhibition analysis (**Supplementary Figure S11**). The UCAA elements in the other two identified aptamers were within non-canonical structural contexts and may only superficially resemble the UCAA motif. Aptamer 80N 142 contained the sequence UCAACU but presents the internal CAAC as the four-nucleotide bulge, rather than the UCAA portion, and both flanking U's are predicted to pair within stems. Nevertheless, this sequence also contained the downstream unpaired U and upstream AC/GU base pairs characteristic of the motif. Although the fourth sequence (80N 433) contained a UCAA motif, it was predicted to present this sequence either as a tetraloop capping an interrupted helix, or as a part of a seven-nucleotide bulge (GUUCAAA), neither of which conforms to the canonical definition of the UCAA.

The (6/5)AL motif is characterized by the presence of six unpaired nucleotides (ARCGUY) opposite five unpaired nucleotides (RARAC) in an asymmetric loop embedded within a stem (**Figure 2C**); where R is any purine and Y is any pyrimidine (28). Of the 16 loop combinations that fit this definition, 6a/5a (AACGUU/GAAAC) and 6b/5b (AGCGUC/AAGAC) variants account for >98% of all (6/5)AL motifs in the 70N round 14 library, along with a small fraction of additional minor variants (28). Searching the candidate sequences for the (6/5)AL motif identified eight sequences that fit the consensus. The 6a/5a variation was present in three sequences (70N 8, 70N 177, and 80N 218). Although most of the previously-identified (6/5)AL aptamers utilize portions of the 80N constant region to form the motif (28), 80N 218 contained the motif entirely within the aptamer's randomized region. Four aptamers containing the 6b/5b variation of the motif were also identified, with two in the common circularly permuted form (70N 89 and 80N 653) and two in the less-common, non-permuted form (70N 105 and 70N 869). A circularly permuted 6c/5b variant that contained the motif within the randomized region was also found (80N 42A). The 6c/5b combination is exceedingly rare, having been previously observed at less than 0.1% of the 70N round 14 population (28). To validate these motif identifications, aptamer:RT 3'

boundary determination and inhibition assays with truncated variants were carried out for two non-circularly permuted (70N 105 and 70N 869) and one circularly-permuted (70N 89) 6b/5b aptamer. All three fully inhibited RT from HIV-1 strain HXB2 when the 3' end was truncated to only three base pairs beyond the asymmetric loop, irrespective of whether the closing stem was Stem I or Stem II (**Supplementary Figures S12–S14**).

Sequences with no obvious motifs were analyzed for their predicted secondary structures. Four of these contained asymmetric internal loops suggestive of (6/5)AL variants that did not conform to the ARCGUY/RARAC consensus sequence and hence escaped detection in the initial sequence-based screening. Two of these contain known, but extremely rare, variations of the motif, including 6a/5d (AACGUU/UAAAC, non-conforming deviations underlined) in 80N 46A29B and 6d/5a (AACGUG/GAAAC) in 70N 24A28B. These sequence combinations were previously detected in a 70N library with frequencies of less than 0.6% (6a/5d) and 0.08% (6d/5a) of all (6/5)AL reads (28). The other two contained previously unobserved variants of the (6/5)AL motif, including the newly-termed 6f/5b (AGCGUA/AAGAC) in 80N 433 – which is flanked by AG/CC closing pairs in Stem I – and 6g/5a (AGCCUC/GAAAC) in 80N 51. The observation of a variant (6/5)AL motif in 80N 433 was especially surprising, as this sequence also contains a non-canonical UCAA bulge, as described above. Minimization of the 80N 433 aptamer, followed by deletion of either the (6/5)AL motif or UCAA bulge, suggested that only the (6/5)AL motif is required for inhibition of HXB2 RT and that the portion containing UCAA is not sufficient for inhibition (**Supplementary Figure S15**).

In total, motif analysis of coenriched and codepleted cluster seed sequences, combined with biochemical validation of a subset of these, identified ten putative F1Pk aptamers, three potential UCAA motif aptamers and twelve (6/5)AL aptamers that include several circular permutations and rare or novel variants. The F1Pk motif comprised the vast majority of the round 14 libraries and continued to dominate populations despite their overall depletion. One aptamer (80N 433) contained both a cryptic (6/5)AL motif and a dispensable, non-canonical UCAA bulge. Ten additional aptamers neither conformed to previously-defined motifs nor showed sequence or structure similarity with each other. We suspect, based on the abundance of the motif-unknown sequences in the nitrocellulose binding populations, that some of these aptamers may be low-fitness species with protein independent enrichment. Overall, Poly-Target selection and coenrichment analysis helped to reduce the lead candidate space by several orders of magnitude to identify highly enriched, rare, and unique genotypes that were present within the pre-enriched round 14 libraries. It is unlikely that low-throughput sequencing would have identified these unknown and previously unobserved sequences, as their relative abundance in each library remained low even after three additional rounds of selection.

Broad-spectrum Inhibition Varies with Aptamer Motif

Coenrichment against multiple, divergently-related protein targets could signal broad-spectrum recognition and inhibition across the panel of RTs. To test this possibility, we assayed the 35 cluster-representing aptamers for inhibition of the DNA-dependent DNA polymerase (DDDP) activity of RT using primer extension assays. Three previously characterized 70N (6/5)AL aptamers (88.1, A9, x1.1) were included as inhibition controls. Aptamers A9 and 88.1 contain a circularly permuted 6b/5b motif and enriched along many selection trajectories, despite being notably absent from sequences obtained here for the round 14 library. Aptamer x1.1 contains a 6a/5a motif and was the most abundant sequence in the 70N round 14 library (28) yet was among the most depleted sequences in the round 17 populations. The vast majority of aptamers containing known motifs robustly inhibited RT from strain HXB2 (**Figure 3A**, top), which is very closely related (98.9%) to the BH10 strain used to pre-enrich these libraries originally (13). In contrast, only three of the aptamers without recognizable structural motifs inhibited RT from HXB2 (70N 11, 70N 55 and 80N 44), suggesting that the other candidates with unknown structures may have been enriched for binding to nitrocellulose, that they bind RT surfaces that do not interfere with DNA polymerization, or that they are selection parasites.

The R277K point mutant of RT from HXB2 served as initial surrogate for evaluating broad-spectrum inhibition. The K277 polymorphism is prevalent among sequenced strains and present in five of the seven RTs used in these selections, so we reasoned that true broad-spectrum aptamers should be able to inhibit the R277K RT. When all 38 aptamers were tested for inhibition of R277K, 18 of these inhibited both HXB2 and R277K (**Figure 3A**, bottom). The (6/5)AL and UCAA motif aptamers demonstrated strong inhibition of R277K, with the exception of 80N 51, which weakly inhibited RT from HXB2 and failed to inhibit the point mutant. This aptamer is a previously unobserved 6g/5a variation of the (6/5)AL motif and experienced a mix of both strong depletion and enrichment, often against the same target in replicate selection trajectories. Its coenrichment may therefore reflect the stochastic nature of the selection rather than a true positive coenrichment signal. Of the three aptamers of unknown structures that inhibit HXB2, only aptamer 80N 44 inhibits R277K. As expected, the F1Pk pseudoknot aptamers uniformly failed to inhibit.

When the 18 aptamers that inhibited both HXB2 and R277K were evaluated for inhibition of the panel of RTs used in the selection (**Figure 3B**), the (6/5)AL and UCAA motif aptamers were consistently broad-spectrum. Among the (6/5)AL aptamers, 70N 89 exhibited robust broad-spectrum inhibition of DDDP activity across the lentiviral RT panel; to a slightly lesser degree aptamers 70N 653 and 88.1 also inhibited broadly across the panel. These three aptamers all carry 6b/5b motifs. Aptamer A9, which also carries a 6b/5b motif, showed less inhibition and greater variability across the panel, potentially due to non-productive contributions of sequences surrounding the motif. Aptamer 70N 105, which carries a non-circularly permuted form of the 6b/5b motif, also exhibited a moderate to strong inhibition profile, as did the 6c/5b variant (80N 42A), which is a single nucleotide change from the 6b/5b motif. Other variations of the (6/5)AL motifs showed no discernible pattern of inhibition across the panel. In particular, 80N 433, which contains both a (6/5)AL and a UCAA motif, behaved most like x1.1 in that it inhibited RTs from 94CY, MVP and EHO. RT from 94CY and EHO were inhibited more or less uniformly by all (6/5)AL aptamers tested, but inhibition was more variable for RTs from 93TH, MVP and TAN1B. Aptamers that carry UCAA motifs inhibited RTs from 94CY and EHO and exhibited mixed behavior against RTs from 93TH and MVP. Aptamer 80N 148 moderately inhibited RT from 93TH, but it failed against RT from MVP, while aptamer 80N 16 demonstrated the opposite pattern. All three UCAA aptamers inhibited RT from HIV-2 (EHO) to an extent that is comparable to that observed for the (6/5)AL aptamers, but they all failed to inhibit RT from TAN1B. The unknown aptamer, 80N 44, was only moderately broad-spectrum, inhibiting RTs from 94CY and EHO RTs, but none of the other RTs from non-subtype B lentiviruses. 3' boundary determination and truncation experiments with 80N 44 against HXB2 RT identify a minimized 54 nucleotide sequence predicted to fold as a stem, interrupted with bulges and a (4/2) asymmetric loop, and capped with a six nucleotide loop (**Supplementary Figure S16**). The control F1Pk aptamers weakly inhibited RT from EHO, which is the only RT outside the HIV-1 subtype B to contain R277, but they failed to inhibit RTs from the other non-subtype B lentiviruses (**Figure 3B**).

Sorting the aptamers by their average RT inhibition reveals a clear correlation of inhibition profiles with secondary structural motifs (**Figure 4**). Taken together, these data indicate that the (6/5)AL and UCAA motifs are capable of inhibiting a broad collection of non-subtype B RTs, and that several 6b/5b variants are capable of robust inhibition against every RT in our selection panel. While the UCAA and unknown motifs show limited inhibition outside of group M, they are potent inhibitors of the M:A and M:B HIV-1 RTs tested here.

Conversion of (6/5)AL variants to the canonical 6b/5b improves RT inhibition

Aptamers 88.1 (6b/5b), 80N 42A (6c/5b), and 80N 433 (6f/5b) all carry 6b/5b motifs or single-nucleotide variations, and they represent a gradient of inhibitory potency against RTs from non-B clades. To assess the relative contributions of nucleotide composition within and outside the asymmetric loop, we

converted aptamer 88.1 from 6b/5b to 6f/5b and 6c/5b (**Figure 5A**) and each of the other two into canonical 6b/5b forms. These modifications are single nucleotide changes to interconvert AGCGUC (6b) to either AGCGUA (6f) or AACGUC (6c), or vice versa. Establishing a canonical 6b/5b structural context for 80N 433 also required an A to G substitution immediately upstream of the 6b element to stabilize the flanking stem. The three original aptamers and the four variants were assayed for inhibition of RTs from HXB2, R277K, and five non-B clades (**Figure 5B**). Conversion of 88.1 away from the 6b/5b variant had little effect on the overall inhibition profile, with the exceptions of partial loss of inhibition for RTs from 93TH and TAN1B. In contrast, conversion of 80N 433 to 6b/5b (80N 433bb) dramatically increased its inhibitory potency, especially for RTs from 93TH, MVP and TAN1B, making 80N 433bb the strongest broad-spectrum inhibitor among all aptamers examined in this study. Conversion of 80N 42A to 6b/5b also improved its performance against the panel, with lowered mean primer extension values, albeit to a lesser degree than for 80N 433. Taken together, these data suggest that the exact composition of the 6 nucleotide bulge of the (6/5)AL loop is important for broad spectrum binding, that flanking sequences contribute directly or indirectly to net inhibition, and that the terminal C of the 6 nucleotide bulge, present in both 6b and 6c variants, may be especially important for establishing productive molecular contacts, particularly for RTs from 93TH and TAN1B.

Broad-Spectrum Aptamers Inhibit Outside of the Selection Panel

We reasoned that aptamers capable of inhibiting phylogenetically diverse RT likely interact with conserved features that would also be present in RTs that were not included in the Poly-Target selection panel. Anti-RT aptamers with broad-spectrum ability are therefore expected to bind and inhibit RTs that were not part of this training set. The aptamers chosen for this analysis were the most potent representatives of the three structural motifs that inhibited outside of subtype B: the 6b/5b converted form of aptamer 80N 433 (80N 433bb), a UCAA aptamer (80N 148) and the putative (4/2)AL motif (80N 44). The RTs for this assay sample two additional subtypes from HIV-1 group M and one from SIV_{CPZ}. The group M RTs included a subtype C (98CN) and a circulating A/D recombinant form (92UG) for which the *pol* gene encoding RT groups within subtype D. Subtype C is the dominant subtype in South and Central Africa and the Asian subcontinent and represents nearly half of all current HIV infections globally (30). The SIV_{CPZ} RT is from the US strain, derived from the chimpanzee species *Pan troglodytes troglodytes* (SIV_{CPZ}*Ptt*). It is more evolutionarily related to HIV-1 group M subtypes than the TAN1B SIV strain used in the selection panel (SIV_{Cpz}*Pts*), which is from the species *Pan troglodytes schweinfurthii* (**Supplementary Figure S1**) (32). Against the RT from subtype D (92UG), the UCAA aptamer showed moderate inhibition and the 6b/5b aptamer showed complete inhibition (**Figure 6**). When assayed against the RT from subtype C (98CN), all three aptamers showed moderate inhibition, with the 6b/5b aptamer exhibiting virtually complete inhibition of the DDDP activity. Finally, only the 6b/5b aptamer inhibited the RT from SIV_{CPZ} (US). These results provide further evidence of the ability of the UCAA and unknown motif to inhibit non-subtype B RTs and of the 6b/5b motif to strongly inhibit RT from phylogenetically diverse lentiviral strains.

Broad-Spectrum Anti-RT Aptamers Bind with Low Nanomolar Affinity

We hypothesized that the observed patterns of sequence enrichment and enzymatic inhibition above should reflect relative affinities for each aptamer-RT combination. For example, because modifying aptamer 80N 433 into a canonical 6b/5b form improved its inhibition of RTs from 93TH and TAN1B RT, the modified aptamer is expected to exhibit improved affinity for these RTs. Apparent dissociation constants for a number of aptamer-RT pairs were determined by a nitrocellulose filter binding assay (**Table 1 and Supplementary Figure S17**). As expected, aptamer 70N 2 (F1Pk) bound well to RT from HXB2 (Kd ≈ 110 nM) but showed no discernable affinity for the R277K point mutant, consistent with its inhibition patterns (**Figure 3A**). Furthermore, its affinity for RT from HXB2 was notably weaker than affinities observed for the broad-spectrum aptamers tested here, consistent with its observed moderate depletion in the HXB2 trajectory and powerful depletion in each of the others (**Figure 2** and **Supplementary Table S5**). Dissociation constants for all of the other aptamers were in the low

nanomolar range (< 100 nM) for binding to HXB2. Because these assays were all performed at the same time using the same protein preparation, we conclude that the affinity of aptamer 80N 433bb for RT from HXB2 is 5-fold improved relative to that of the pseudoknot aptamer 70N 2. All of the broad-spectrum aptamers showed reduced affinity for the R277K mutant, relative to their affinities for RT from HXB2. For the RT's from non-subtype B lentiviruses, relative binding affinities among the broad-spectrum aptamers correlated with their inhibition profiles. In particular, Kd values for the 6b/5b variant of 80N 433 were in the low nanomolar range across the RT panel, and this aptamer uniformly bound more strongly to each RT than did any of the other aptamers. Affinity improvements associated with converting the original 80N 433 from 6f/5b to 6b/5b ranged from approximately 3-fold for HXB2 and 93TH to 13-fold for TAN1B, illustrating the variable contributions of these nucleotide changes upon the RT-aptamer interactions.

Broad-Spectrum Anti-RT Aptamers Suppress Viral Replication in Cell Culture Assays

A target application of broad-spectrum RNA aptamers is to suppress productive replication of diverse viruses or emergent and potentially resistant forms. Therefore, to determine whether aptamers that demonstrate broad-spectrum activity *in vitro* also inhibit diverse HIV in a biological context, we adapted an assay that we had previously developed for monitoring aptamer-mediated inhibition of HIV replication in cell culture (18, 19, 36). Briefly, transfection of plasmids encoding a replication-deficient HIV reporter virus and the glycoprotein from vesicular stomatitis virus (VSV-G) leads to production of virus that are competent for a single cycle of replication and for which transfection and infection efficiencies can both be measured using the virally-encoded EGFP. Cotransfection of aptamer-expressing plasmid simultaneously with viral plasmids can lead to packaging of the aptamer into the virus during assembly, inhibition of reverse transcription in the target cells, and loss of infectivity that can be measured by a loss of fluorescence signal in the target cells. To incorporate phylogenetically diverse RT subtypes into this assay, we first built and evaluated proviral plasmids to express several RTs from our Poly-Target selection panel (HXB2, R277K, 93TH, 94CY, and MVP) such that only the RT segments differed in each construct (19). This assay was used to evaluate viral inhibition by aptamers that demonstrated broad-spectrum RT inhibition *in vitro* by co-transfecting various combinations of proviral and helper VSV-G plasmids with aptamer or control plasmids, collecting the pseudotyped virus, and determining the percent of EGFP-positive cells after infection of fresh 293FT cells (**Figure 7**). Infectivity was normalized to p24 levels determined by ELISA. As observed previously (19), aptamer 70.05 (an F1Pk pseudoknot) strongly inhibited infectivity of virus carrying the HXB2 RT, but not the R277K point mutant or any of the non-subtype B RTs. In contrast, aptamers 80N 433 and 80N 433bb inhibited infectivity of all recombinant viruses in the panel. Aptamers 80N 148 and 80N 44 demonstrated a variable pattern against the non-subtype B RTs. Both inhibited replication by viruses carrying RT from 94CY but only 80N 148 inhibited virus carrying RT from 93TH, even though the RTs from 94CY and 93TH both group within subtype A and are 91.4% identical (98.2% similar). Neither 80.148 nor 80.44 inhibited viruses carrying RT from the MVP5180 strain of HIV-1 Group O. These results are consistent with our biochemical inhibition results and closely mirror our previous observations for inhibition by the major anti-RT motifs in cell culture (19).

DISCUSSION

Recent advances in aptamer technology have enabled increased selection throughput and high-resolution analysis of selection outcomes (37, 38). Microfluidic (39) and multiplexed selection platforms (40, 41) facilitate efficient and simultaneous selections against numerous targets, and emulsion methods that encapsulate single genotypes into "monoclonal aptamer particles" readily partition or sort according to phenotype (42, 43). Post-selection, high-throughput sequencing (HTS) has empowered optimization of candidate aptamers based on round-to-round enrichment of sequences and by providing large data sets that allow for powerful bioinformatic analyses of sequence:structure:function relationships (28, 44-46). In addition to advances in selection methodology and candidate identification, high-throughput aptamer characterization platforms that utilize microarrays can screen thousands of

aptamers simultaneously (47) and directly link genotype to phenotype when performed on a sequencing platform (48, 49). Here we sought to combine HTS with multiplexed selections against a diverse panel of recombinant RTs. We applied these technologies to elicit specialized binding and inhibition phenotypes (cross-reactivity) from well-characterized and pre-enriched aptamer libraries. Furthermore, we sequenced negative selection populations and performed our positive selections in duplicate. The combination enabled coenrichment analysis of multiple selection trajectories, nuanced with data from duplicate and negative selections. This strategy efficiently narrowed the number of potential candidates to an examinable amount, allowing us to identify highly-potent RNA broad-spectrum inhibitors of lentiviral RTs among these candidates.

Other selection approaches have previously been used to identify cross-reactive aptamers or to exploit branched selections. In “toggle SELEX” (50), the target of a single-selection trajectory is alternated, or “toggled” between rounds; this approach was used to identify inhibitors of human and porcine thrombin and later to identify broadly-reactive aptamers targeting whole bacterial cells (51). In another approach, single-pot selections against numerous targets were used to identify cross-reactive aptamers against several M-types of *Streptococcus pyogenes* (52) and against HA proteins from multiple strains of Influenza A (53). Although both of these methods are powerful (alternating or simultaneous targets), they rely on a single evolutionary trajectory and lack the target-specific information that can inform the aptamer selection and design process. Recently, Dupont *et al*. reported on a clever branched selection approach against alanine point mutants of serpin plasminogen activator inhibitor-1 (PAI-1) (54). Utilizing a library previously selected against wild type PAI-1, those authors performed one additional round of selection against a panel of 10 targets, in parallel, followed by high-throughput sequencing, to identify aptamer binding site preferences. Unlike the Poly-Target selection described here, the pre-enriched library utilized by Dupont *et al*. had not been saturated. In the original selection against PAI-1, enrichment of the library was detected after 5 rounds and proceeded for a total of 8 rounds (55). Rather than using the heavily-enriched library from round 8, the branched selection began with round 5, allowing for a greater diversity of aptamers to emerge.

The Poly-Target approach utilized pre-enriched libraries to simultaneously explore a wider sequence space than available in a traditional aptamer directed evolution strategy. Interestingly, neither abundance, enrichment nor coenrichment alone was a strong predictor of fitness in the Poly-Target selection performed here. Highly abundant sequences in the starting libraries depleted across most selection trajectories yet remained as dominant species within the round 17 populations. In contrast, most of the 6b/5b variants that enriched through the selection were so rare in the starting populations that, despite their large fold-enrichment, they remained as a relatively small percentage of the populations and could only be reliably identified through HTS. Coenrichment was slightly more predictive of broad-spectrum phenotypes after removing aptamers that enriched against nitrocellulose alone. Nevertheless, several F1Pk aptamers demonstrated enrichment across several trajectories despite their lack of broad-spectrum inhibition. The combined use of coenrichment and codepletion analysis of sequence clusters identified sequences that experienced mixed enrichment and depletion, either across trajectories or between replicates. The most productive analytic strategy for the present datasets combined each of these approaches with careful curation based on sequence and structural motifs established from previous investigations. The Poly-Target approach may be broadly applicable for any combinatorial selection or directed evolution strategy that seeks to identify broad-spectrum behavior given an appropriate phenotypic screen.

Our selection strategy was designed to intentionally select for promiscuity against a family of related targets, rather than specificity for a single target or its point-mutants, and it relied on the sequencing depth provided by HTS to identify functionally rare aptamers that enriched from our round 14 starting libraries. We developed and utilized a coenrichment analysis strategy to efficiently reduce the dataset from over a hundred million sequences to focus on dozens of candidate sequence clusters for further

analysis. We were able to identify several rare variants of (6/5)AL motifs and also a previously-unknown aptamer inhibitor of HIV-1 M subtype RTs. Inhibition assays identified the 6b/5b variant of the (6/5)AL motif as an especially potent inhibitor of the DDDP activity of RTs utilized in the selection panel and several RTs that were not included in the selection. Conversion of aptamer 80N 433 towards the 6b/5b motif improved its inhibition profile across the panel of RTs and most notably against 93TH, MVP and TAN1B. Furthermore, the UCAA aptamer (80N 148) and aptamer 80N 44 demonstrated inhibition of RT outside of subtype B strains. Follow-up assays correlated inhibition of RTs with binding affinity and suppression of viral replication. As our efforts were focused on identification of broad-spectrum inhibitors, we did not attempt to find strain-specific inhibitors nor did we closely examine the role of individual nucleotides and their interactions with specific RTs. The wealth of data provided by the Poly-Target selection approach should, in principle, allow one to look for enrichment exclusive for a particular target, in addition to advancing the broad-spectrum objectives that were the focus of the present study.

MATERIAL AND METHODS

RT Expression and Purification

DNA encoding the p66 and p51 subunits of each RT (**Supplementary Table S1**) were PCR amplified from previously described pET200/D-TOPO expression vectors (22). Amplicons were then restriction digest cloned into the pRT-Dual plasmid, a derivative of pETDuet-1 vector (a gift from Stefan Sarafianos (56)). Plasmids expressing RTs from HXB2, R277K, 94CY and TAN1B utilized the PpuM1/SacI cloning sites for the p51 subunit, and the SacII/AvrII sites for the p66 subunit ("pRTD" series plasmids). Whereas RTs from 93TH, MVP and EHO utilized the same restriction sites for the p66 subunit but utilized NotI/SalI for the p51 subunit ("pRTD2" series plasmids). Additional plasmid engineering was performed on the ribosome binding site upstream of the p66 subunit in the pRTD2 series plasmids to optimize expression. Plasmid were confirmed by Sanger sequencing (University of Missouri DNA Core Facility) and are available upon request.

RT expression plasmids were heat shock transformed into *E. coli* BL21(DE3)pLysS competent cells and then incubated overnight at 37° C on LB-Agar plates supplemented with selective antibiotic (50 µg/mL streptomycin). Clonal isolates from each plate were recovered and incubated for approximately 16 hours at 37° C with 250 RPM shaking in 10 mL of 2xYT selective liquid media. Cultures were then diluted into 1 L of fresh media and optical density at 600 nm was monitored until reaching 0.5, whereupon protein overexpression was induced with 1 mM IPTG. Following a 4-hour incubation, samples were centrifuged for 15 minutes at 4,000 RCF. Supernatants were decanted and cell pellets were frozen at -80° C until purification. For purification, cell pellets were resuspended in sonication buffer (25 mM Tris-HCl pH 8.0, 500 mM NaCl, 1 mM PMSF, 0.15 mg/mL lysozyme) and then subjected to four ultrasonication steps of 30 seconds, on ice, with 2 minutes of rest in between steps. Cell lysates were then centrifuged for 15 minutes at 4° C and 12,000 RCF to remove cell debris. Cell extracts were then passed through a 0.45 µm filter to remove insoluble material and applied to a Ni-NTA agarose affinity column (Qiagen) for His tag purification. Purification was performed according to the manufacturer's protocol, with an added high salt wash (2 M NaCl) to remove any endogenous nucleic acids bound to RTs. Eluted protein samples were pooled and quantified using UV absorbance at 280 nm on a NanoDrop 1000 spectrophotometer (Thermo Fisher) with estimated extinction coefficient and molecular weight information. Purified proteins were concentrated using Amicon Ultra Centrifugal Filters (Millipore Sigma) and dialyzed into 2x storage buffer (100 mM HEPES pH 7.5, 100 mM NaCl) using Slide-A-Lyzer cassettes (Thermo Scientific). RT preps were validated for purity and size by SDS-PAGE, and for activity by comparison of primer extension assays against previous preps. Proteins were stored at -20° C after addition of glycerol to 50% (v/v).

Poly-Target Selection

cDNAs corresponding to the pre-enriched 70N and 80N aptamer libraries (13) were transcribed using T7 RNA polymerase, *in vitro* transcription buffer (50 mM Tris-HCl pH 7.5, 15 mM $MgCl_2$, 5 mM DTT,

and 2 mM spermidine), and 2 mM of each ATP, CTP, GTP and UTP. Reactions were incubated at 37° C for a minimum of 4 hours and halted with the addition of gel loading buffer (95% formamide, 5mM EDTA, with trace amounts of xylene cyanol FF and bromophenol blue). Transcribed RNAs were purified through denaturing polyacrylamide gel electrophoresis (6% TBE-PAGE, 8 M urea) and bands corresponding to the expected size were gel extracted and eluted while tumbling overnight in 300 mM Sodium Acetate pH 5.4. Eluates were ethanol precipitated, resuspended in TE buffer (10 mM Tris-HCl pH 8.0, 1 mM EDTA), and stored at -20° C until use. RNA concentrations were determined on a NanoDrop 1000 spectrophotometer (Thermo Fisher). For each trajectory and round of selection, 200 pmol of the transcribed libraries were resuspended in 100 µL binding buffer (150 mM KCl, 10 mM $MgCl_2$, 50 mM Tris-HCl pH 7.5) and renatured by heating to 65 °C and cooling on ice. 40 pmol of the respective RT was then added, and the mixture was incubated on ice for an additional 20 minutes. Separately, a 25 mm nitrocellulose filter (#HAWP02500, Millipore Sigma) was pre-wet with 2 mL binding buffer on a sampling manifold (#XX2702550, Millipore Sigma). Immediately before application of incubated RNA:RT complex, the nitrocellulose filter was washed again with 1 mL of binding buffer under applied vacuum. RNA:RT complex was then applied to filter under vacuum and washed with 1 mL of binding buffer. Suction continued for 10 minutes. The filter was then removed and incubated in extraction buffer (8 M urea, 50 mM NaCl, 10 mM EDTA). RNA was recovered by phenol:chloroform extraction of the filter and ethanol precipitation. Recovered RNA was reverse transcribed using ImProm-II Reverse Transcriptase (Promega) and PCR amplified to repeat the selection process, or for high-throughput sequencing (see below). Prior to round 15, transcribed round 14 libraries were incubated with a thin strip of nitrocellulose for several minutes to subtract non-specific binders and RNA was extracted and purified as described above, with the exclusion of the RT binding and partitioning steps. Nitrocellulose-binding RNAs were recovered and reverse transcribed for HTS, while nitrocellulose-subtracted RNAs were used for independent selections.

High-throughput Sequencing and Bioinformatics Analysis

Libraries were prepared for sequencing using a series of PCR steps to add Illumina adapters and sequencing indices for multiplexing of the 70N and 80N libraries as previously described (28). Sequencing was performed on an Illumina HiSeq2000 (University of Missouri DNA Core Facility). Populations were demultiplexed to identify and parse the 5' and 3' constant regions. Data pre-processing was performed using cutadapt (57) to trim 5' and 3' constant regions from sequences and to discard any uncut sequences or sequences not within ± 3 of the expected size (70 or 80) after trimming. Trimmed sequences were then filtered for high-quality reads using FASTQ quality filter from the FASTX-Toolkit (http://hannonlab.cshl.edu/fastx_toolkit/). Quality filtering eliminated a sequence if a single position had a Phred quality score of less than 20. Trimmed and quality filtered sequences were then processed using the FASTAptamer toolkit (33) to count and normalize sequence reads (FASTAptamer-Count), calculate fold-enrichment from round 14 to round 17 (FASTAptamer-Enrich), compare sequence frequencies across populations (FASTAptamer-Compare), group related sequences into clusters (FASTAptamer-Cluster) and search for known sequence motifs (FASTAptamer-Search). Custom scripts (open source and available at https://github.com/FASTAptamer/PolyTarget) were written in Perl to perform coenrichment analysis, to map sequences onto their round 14 identity, and to recluster the sequences as described in the results. RNA secondary structures were predicted using the Mfold webserver (35) and depicted using VARNA: Visualization Applet for RNA (58).

Aptamer Generation

Oligonucleotides for DNA transcription templates were ordered from Integrated DNA Technologies and ligated as previously described (59). Ligated oligonucleotides were then PCR amplified with Pfu DNA polymerase and primers containing the T7 promoter and the remainder of the constant region that was not included in the oligonucleotides. Amplification products were verified for size using agarose gel electrophoresis. Run-off transcription reactions using T7 RNA polymerase and RNA extraction and

purification were performed as described above for transcription of Poly-Target libraries. RNAs were refolded by heating to 65° C and cooling on ice prior to use.

Primer Extension Assays

DNA-dependent DNA polymerase activities of RTs were assayed using a 31 nucleotide DNA template (5' CCATAGATAGCATTGGTGCTCGAACAGTGAC 3') and a complementary, 5'-Cy3-labeled 18-nucleotide DNA primer (5' Cy3-GTCACTGTTCGAGCACCA 3') as previously described (29). In short, 20 nM of RT and 100 nM of aptamer (omitted for "*No Aptamer*" control) were pre-incubated on ice for 10 minutes in extension buffer (50 mM Tris-HCl pH 7.5, 50 mM NaCl, 5 mM $MgCl_2$). 10 nM primer, 20 nM template and 100 μM of each dNTP were then added immediately before incubation at 37° C for 10 minutes. Reactions were halted with the addition of gel loading buffer (95% formamide, 5 mM EDTA, with trace amounts of xylene cyanol FF and bromophenol blue) and analyzed by denaturing polyacrylamide gel electrophoresis (10% TBE-PAGE, 8 M urea). Gels were scanned on a Typhoon FLA9000 imager (GE Healthcare) and quantified using Multi Gauge software (Fujifilm) for fraction of primer extended. Primer extension values were then normalized by subtracting the mean "*No RT*" value for the respective RT and multiplying by a normalization factor that defines 100% extension as the mean extension in the "*No Aptamer*" control.

Aptamer:RT 3' Boundary Determination

In vitro transcribed and purified RNA was treated with Antarctic phosphatase (Fermentas) to remove the 5' terminal phosphate and subsequently labeled with T4 polynucleotide kinase in the presence of γ-^{32}P labeled ATP (Perkin Elmer). Radiolabeled RNA was gel purified by denaturing PAGE as described for transcription of libraries. RNase T1 digestion was performed by incubating thermally renatured RNA (> 10^6 CPM) with 40 units of RNase T1 (Thermo Fisher) in digestion buffer (25 mM sodium citrate pH 5.0, 6 M urea) for 5 minutes at 55° C. T1 digestion was halted with the addition of gel loading buffer. Alkaline hydrolysis was performed by incubating RNA in 50 mM sodium carbonate pH 9.0 at 90° C for 10 minutes. Hydrolysis was halted upon addition of 300 mM sodium acetate pH 5.0 and were then ethanol precipitated and resuspended in H_2O. Aptamer:RT 3' boundary was determined by incubating 50 pmol RNA with 100 pmol HXB2 RT and partitioning the bound complexes as described above for the Poly-Target selection. RNAs were recovered from the filter and resolved on a denaturing polyacrylamide gel (15% TBE-PAGE, 8 M urea).

Affinity Constant Determination

Affinity constants (K_d's) were determined by a radiolabeled binding assay. Approximately 15-20k CPM of labeled and refolded RNA was incubated with varying concentrations of RT (0.1 – 1000 nM, or without RT to determine background binding) in binding buffer (50 mM Tris-HCl pH 7.5, 140 mM KCl, 1 mM $MgCl_2$, 0.1 μg/mL bovine serum albumin) and allowed to equilibrate on ice for 15 minutes. Assembled RNA:RT complexes were then partitioned from unbound RNA by passing samples over a nitrocellulose filter (#HAWP02500, Millipore Sigma) under vacuum (#XX2702550, Millipore Sigma) and immediately washing with 500 μL binding buffer. Radioactivity retained on filters was counted by adding 4 mL of scintillation fluid to filters placed inside of scintillation vials and counted using a liquid scintillation counter. Fraction of RNA bound was calculated by determining the fraction of radioactivity bound and were fit to a one site, specific binding curve using Prism GraphPad 6.2.

Viral Infectivity Assay

Cell culture, virus production and evaluation of viral infectivity were carried out as previously described (19, 36). Single-cycle infectivity assays using aptamer-expressing plasmids, pNL4-3-CMV-GFP and pMD-G (VSV-G), were performed by transfecting 293FT cells with polyethylenimine (PEI) in six-well cell culture dishes. All transfections were performed on cells plated the previous day (50% confluence) using PEI at 3 μl/μg DNA, as previously described. Aptamer-expressing plasmids (1000 ng) were co-transfected with a mixture of pNL4-3-CMV-GFP (150 ng) and pMD-G (50 ng). The medium was

changed approximately 12 hours after transfection. Viral supernatant was harvested 48 hours after the post-transfection media change and clarified by centrifugation to remove cellular debris. Cell-free viral supernatant (50 µl) was added to fresh 293FT cells to determine infectivity. Infected cells were collected 24-48 hours post-infection, fixed with 4% paraformaldehyde and analyzed on an Accuri C6 Flow Cytometer (BD Biosciences) to determine the percentage of infected (EGFP-positive) cells. Infectivity data was normalized to levels of p24 determined by ELISA.

FUNDING

This work was supported by National Institutes of Health grant R01AI074389 to D.H.B. and by a graduate research assistantship to K.K.A. from the University of Missouri Department of Biochemistry.

ACKNOWLEDGEMENTS

The authors would like to thank Katherine N. Wilsdon for technical assistance.

REFERENCES

1. Lloyd,S.B., Kent,S.J. and Winnall,W.R. (2014) The High Cost of Fidelity. *AIDS Res. Hum. Retroviruses*, **30**, 8–16.2. Schlub,T.E., Grimm,A.J., Smyth,R.P., Cromer,D., Chopra,A., Mallal,S., Venturi,V., Waugh,C., Mak,J. and Davenport,M.P. (2014) Fifteen to twenty percent of HIV substitution mutations are associated with recombination. *J. Virol.*, **88**, 3837–3849.

3. Cuevas,J.M., Geller,R., Garijo,R., López-Aldeguer,J. and Sanjuán,R. (2015) Extremely High Mutation Rate of HIV-1 In Vivo. *PLoS Biol.*, **13**, e1002251.

4. Wainberg,M.A., Zaharatos,G.J. and Brenner,B.G. (2011) Development of antiretroviral drug resistance. *N. Engl. J. Med.*, **365**, 637–646.

5. Hu,W.S. and Hughes,S.H. (2012) HIV-1 Reverse Transcription. *Cold Spring Harbor Perspect. Med.*, **2**, a006882.

6. Günthard,H.F., Saag,M.S., Benson,C.A., del Rio,C., Eron,J.J., Gallant,J.E., Hoy,J.F., Mugavero,M.J., Sax,P.E., Thompson,M.A., *et al.* (2016) Antiretroviral Drugs for Treatment and Prevention of HIV Infection in Adults: 2016 Recommendations of the International Antiviral Society-USA Panel. *JAMA*, **316**, 191–210.

7. Deeks,S.G., Lewin,S.R., Ross,A.L., Ananworanich,J., Benkirane,M., Cannon,P., Chomont,N., Douek,D., Lifson,J.D., Lo,Y.R., *et al.* (2016) International AIDS Society global scientific strategy: towards an HIV cure 2016. *Nat. Med.*, **22**, 839–850.

8. Tuerk,C. and Gold,L. (1990) Systematic evolution of ligands by exponential enrichment: RNA ligands to bacteriophage T4 DNA polymerase. *Science*, **249**, 505–510.

9. Ellington,A.D. and Szostak,J.W. (1990) In vitro selection of RNA molecules that bind specific ligands. *Nature*, **346**, 818–822.

10. Li,Y. (2015) A Quarter Century of In Vitro Selection. *J. Mol. Evol.*, **81**, 137–139.

11. Tuerk,C., MacDougal,S. and Gold,L. (1992) RNA pseudoknots that inhibit human immunodeficiency virus type 1 reverse transcriptase. *Proc. Natl. Acad. Sci. U.S.A.*, **89**, 6988–6992.

12. Green,L., Waugh,S., Binkley,J.P., Hostomska,Z., Hostomsky,Z. and Tuerk,C. (1995) Comprehensive Chemical Modification Interference and Nucleotide Substitution Analysis of an RNA Pseudoknot Inhibitor to HIV-1 Reverse Transcriptase. *J. Mol. Biol.*, **247**, 60–68.

13. Burke,D.H., Scates,L., Andrews,K. and Gold,L. (1996) Bent Pseudoknots and Novel RNA Inhibitors of Type 1 Human Immunodeficiency Virus (HIV-1) Reverse Transcriptase. *J. Mol. Biol.*, **264**, 650–666.

14. Held,D.M., Kissel,J.D., Saran,D., Michalowski,D. and Burke,D.H. (2006) Differential susceptibility of HIV-1 reverse transcriptase to inhibition by RNA aptamers in enzymatic reactions monitoring specific steps during genome replication. *J. Biol. Chem.*, **281**, 25712–25722.

15. Joshi,P. and Prasad,V.R. (2002) Potent Inhibition of Human Immunodeficiency Virus Type 1 Replication by Template Analog Reverse Transcriptase Inhibitors Derived by SELEX (Systematic Evolution of Ligands by Exponential Enrichment). *J. Virol.*, **76**, 6545–6557.

16. Chaloin,L., Lehmann,M.J., Sczakiel,G. and Restle,T. (2002) Endogenous expression of a high-affinity pseudoknot RNA aptamer suppresses replication of HIV-1. *Nucleic Acids Res.*, **30**, 4001–4008.

17. Joshi,P.J., North,T.W. and Prasad,V.R. (2005) Aptamers directed to HIV-1 reverse transcriptase display greater efficacy over small hairpin RNAs targeted to viral RNA in blocking HIV-1 replication. *Mol. Ther.*, **11**, 677–686.

18. Lange,M.J., Sharma,T.K., Whatley,A.S., Landon,L.A., Tempesta,M.A., Johnson,M.C. and Burke,D.H. (2012) Robust Suppression of HIV Replication by Intracellularly Expressed Reverse Transcriptase Aptamers Is Independent of Ribozyme Processing. *Mol. Ther.*, **20**, 2304–2314.

19. Lange,M.J., Nguyen,P.D.M., Callaway,M.K., Johnson,M.C. and Burke,D.H. (2017) RNA-protein interactions govern antiviral specificity and encapsidation of broad spectrum anti-HIV reverse transcriptase aptamers. *Nucleic Acids Res.*, **45**, 6087–6097.

20. Jaeger,J., Restle,T. and Steitz,T.A. (1998) The structure of HIV-1 reverse transcriptase complexed with an RNA pseudoknot inhibitor. *EMBO J.*, **17**, 4535–4542.

21. Kensch,O., Connolly,B.A., Steinhoff,H.-J., McGregor,A., Goody,R.S. and Restle,T. (2000) HIV-1 reverse transcriptase-pseudoknot RNA aptamer interaction has a binding affinity in the low picomolar range coupled with high specificity. *J. Biol. Chem.*, **275**, 18271–18278.

22. Held,D.M., Kissel,J.D., Thacker,S.J., Michalowski,D., Saran,D., Ji,J., Hardy,R.W., Rossi,J.J. and Burke,D.H. (2007) Cross-Clade Inhibition of Recombinant Human Immunodeficiency Virus Type 1 (HIV-1), HIV-2, and Simian Immunodeficiency Virus SIVcpz Reverse Transcriptases by RNA Pseudoknot Aptamers. *J. Virol.*, **81**, 5375–5384.

23. Schneider,D.J., Feigon,J., Hostomsky,Z. and Gold,L. (1995) High-affinity ssDNA inhibitors of the reverse transcriptase of type 1 human immunodeficiency virus. *Biochemistry*, **34**, 9599–9610.

24. Kissel,J.D., Held,D.M., Hardy,R.W. and Burke,D.H. (2007) Single-Stranded DNA Aptamer RT1t49 Inhibits RT Polymerase and RNase H Functions of HIV Type 1, HIV Type 2, and SIVCPZ RTs. *AIDS Res. Hum. Retroviruses*, **23**, 699–708.

25. Kissel,J.D., Held,D.M., Hardy,R.W. and Burke,D.H. (2007) Active site binding and sequence requirements for inhibition of HIV-1 reverse transcriptase by the RT1 family of single-stranded DNA aptamers. *Nucleic Acids Res.*, **35**, 5039–5050.

26. Michalowski,D., Chitima-Matsiga,R., Held,D.M. and Burke,D.H. (2008) Novel bimodular DNA aptamers with guanosine quadruplexes inhibit phylogenetically diverse HIV-1 reverse transcriptases. *Nucleic Acids Res.*, **36**, 7124–7135.

27. Ditzler,M.A., Bose,D., Shkriabai,N., Marchand,B., Sarafianos,S.G., Kvaratskhelia,M. and Burke,D.H. (2011) Broad-spectrum aptamer inhibitors of HIV reverse transcriptase closely mimic natural substrates. *Nucleic Acids Res.*, **39**, 8237–8247.

28. Ditzler,M.A., Lange,M.J., Bose,D., Bottoms,C.A., Virkler,K.F., Sawyer,A.W., Whatley,A.S., Spollen,W., Givan,S.A. and Burke,D.H. (2013) High-throughput sequence analysis reveals structural diversity and improved potency among RNA inhibitors of HIV reverse transcriptase. *Nucleic Acids Res.*, **41**, 1873–1884.

29. Whatley,A.S., Ditzler,M.A., Lange,M.J., Biondi,E., Sawyer,A.W., Chang,J.L., Franken,J.D. and Burke,D.H. (2013) Potent Inhibition of HIV-1 Reverse Transcriptase and Replication by Nonpseudoknot, 'UCAA-motif' RNA Aptamers. *Mol. Ther. Nucleic Acids*, **2**, e71.

30. Hemelaar,J., Gouws,E., Ghys,P.D. and Osmanov,S. (2011) Global trends in molecular epidemiology of HIV-1 during 2000–2007. *AIDS*, **25**, 679–689.

31. Hemelaar,J. (2012) The origin and diversity of the HIV-1 pandemic. *Trends Mol. Med.*, **18**, 182–192.

32. Sharp,P.M. and Hahn,B.H. (2011) Origins of HIV and the AIDS Pandemic. *Cold Spring Harbor Perspect. Med.*, **1**, a006841.

33. Alam,K.K., Chang,J.L. and Burke,D.H. (2015) FASTAptamer: A Bioinformatic Toolkit for High-throughput Sequence Analysis of Combinatorial Selections. *Mol. Ther. Nucleic Acids*, **4**, e230.

34. Spill,F., Weinstein,Z.B., Shemirani,A.I., Ho,N., Desai,D. and Zaman,M.H. (2016) Controlling uncertainty in aptamer selection. *Proc. Natl. Acad. Sci. U.S.A.*, **113**, 12076–12081.

35. Zuker,M. (2003) Mfold web server for nucleic acid folding and hybridization prediction. *Nucleic Acids Res.*, **31**, 3406–3415.

36. Lange,M.J. and Burke,D.H. (2014) Screening inhibitory potential of anti-HIV RT RNA aptamers. *Methods Mol. Biol.*, **1103**, 11–29.

37. Ozer,A., Pagano,J.M. and Lis,J.T. (2014) New Technologies Provide Quantum Changes in the Scale, Speed, and Success of SELEX Methods and Aptamer Characterization. *Mol. Ther. Nucleic Acids*, **3**, e183.

38. Gotrik,M.R., Feagin,T.A., Csordas,A.T., Nakamoto,M.A. and Soh,H.T. (2016) Advancements in Aptamer Discovery Technologies. *Acc. Chem. Res.*, **49**, 1903–1910.

39. Dembowski,S.K. and Bowser,M.T. (2018) Microfluidic methods for aptamer selection and characterization. *Analyst*, **143**, 21–32.

40. Latulippe,D.R., Szeto,K., Ozer,A., Duarte,F.M., Kelly,C.V., Pagano,J.M., White,B.S., Shalloway,D., Lis,J.T. and Craighead,H.G. (2013) Multiplexed Microcolumn-Based Process for Efficient Selection of RNA Aptamers. *Anal. Chem.*, **85**, 3417–3424.

41. Reinholt,S.J., Ozer,A., Lis,J.T. and Craighead,H.G. (2016) Highly Multiplexed RNA Aptamer Selection using a Microplate-based Microcolumn Device. *Sci. Rep.*, **6**, 29771.

42. Wang,J., Gong,Q., Maheshwari,N., Eisenstein,M., Arcila,M.L., Kosik,K.S. and Soh,H.T. (2014) Particle Display: A Quantitative Screening Method for Generating High-Affinity Aptamers. *Angew. Chem.*, **126**, 4896–4901.

43. Gotrik,M., Sekhon,G., Saurabh,S., Nakamoto,M., Eisenstein,M. and Soh,H.T. (2018) Direct Selection of Fluorescence-Enhancing RNA Aptamers. *J. Am. Chem. Soc.*, **140**, 3583–3591.

44. Cho,M., Xiao,Y., Nie,J., Stewart,R., Csordas,A.T., Oh,S.S., Thomson,J.A. and Soh,H.T. (2010) Quantitative selection of DNA aptamers through microfluidic selection and high-throughput sequencing. *Proc. Natl. Acad. Sci. U.S.A.*, **107**, 15373–15378.

45. Berezhnoy,A., Stewart,C.A., McNamara,J.O.,II, Thiel,W., Giangrande,P., Trinchieri,G. and Gilboa,E. (2012) Isolation and Optimization of Murine IL-10 Receptor Blocking Oligonucleotide Aptamers Using High-throughput Sequencing. *Mol. Ther.*, **20**, 1242–1250.

46. Thiel,W.H., Bair,T., Peek,A.S., Liu,X., Dassie,J., Stockdale,K.R., Behlke,M.A., Miller,F.J. and Giangrande,P.H. (2012) Rapid Identification of Cell-Specific, Internalizing RNA Aptamers with Bioinformatics Analyses of a Cell-Based Aptamer Selection. *PLoS ONE*, **7**, e43836.

47. Cho,M., Oh,S.S., Nie,J., Stewart,R., Eisenstein,M., Chambers,J., Marth,J.D., Walker,F., Thomson,J.A. and Soh,H.T. (2013) Quantitative selection and parallel characterization of aptamers. *Proc Natl Acad Sci U S A*, **110**, 18460–18465.

48. Tome,J.M., Ozer,A., Pagano,J.M., Gheba,D., Schroth,G.P. and Lis,J.T. (2014) Comprehensive analysis of RNA-protein interactions by high-throughput sequencing–RNA affinity profiling. *Nat. Meth.*, **11**, 683–688.

49. Buenrostro,J.D., Araya,C.L., Chircus,L.M., Layton,C.J., Chang,H.Y., Snyder,M.P. and Greenleaf,W.J. (2014) Quantitative analysis of RNA-protein interactions on a massively parallel array reveals biophysical and evolutionary landscapes. *Nat. Biotechnol.*, **32**, 562–568.

50. White,R., Rusconi,C., Scardino,E., Wolberg,A., Lawson,J., Hoffman,M. and Sullenger,B. (2001) Generation of species cross-reactive aptamers using 'toggle' SELEX. *Mol. Ther.*, **4**, 567–573.

51. Song,M.Y., Nguyen,D., Hong,S.W. and Kim,B.C. (2017) Broadly reactive aptamers targeting bacteria belonging to different genera using a sequential toggle cell-SELEX. *Sci. Rep.*, **7**, 43641.

52. Hamula,C.L.A., Le,X.C. and Li,X.F. (2011) DNA Aptamers Binding to Multiple Prevalent M-Types of Streptococcus pyogenes. *Anal. Chem.*, **83**, 3640–3647.

53. Shiratori,I., Akitomi,J., Boltz,D.A., Horii,K., Furuichi,M. and Waga,I. (2014) Selection of DNA aptamers that bind to influenza A viruses with high affinity and broad subtype specificity. *Biochem. Biophys. Res. Commun.*, **443**, 37–41.

54. Dupont,D.M., Larsen,N., Jensen,J.K., Andreasen,P.A. and Kjems,J. (2015) Characterisation of aptamer–target interactions by branched selection and high-throughput sequencing of SELEX pools. *Nucleic Acids Res.*, **43**, e139.

55. Madsen,J.B., Dupont,D.M., Andersen,T.B., Nielsen,A.F., Sang,L., Brix,D.M., Jensen,J.K., Broos,T., Hendrickx,M.L.V., Christensen,A., *et al.* (2010) RNA aptamers as conformational probes and regulatory agents for plasminogen activator inhibitor-1. *Biochemistry*, **49**, 4103–4115.

56. Michailidis,E., Marchand,B., Kodama,E.N., Singh,K., Matsuoka,M., Kirby,K.A., Ryan,E.M., Sawani,A.M., Nagy,E., Ashida,N., *et al.* (2009) Mechanism of Inhibition of HIV-1 Reverse Transcriptase by 4'-Ethynyl-2-fluoro-2'-deoxyadenosine Triphosphate, a Translocation-defective Reverse Transcriptase Inhibitor. *J. Biol. Chem.*, **284**, 35681–35691.

57. Martin,M. (2011) Cutadapt removes adapter sequences from high-throughput sequencing reads. *EMBnet.journal*, **17**, pp. 10–12.

58. Darty,K., Denise,A. and Ponty,Y. (2009) VARNA: Interactive drawing and editing of the RNA secondary structure. *Bioinformatics*, **25**, 1974–1975.

59. Alam,K.K., Tawiah,K.D., Lichte,M.F., Porciani,D. and Burke,D.H. (2017) A Fluorescent Split Aptamer for Visualizing RNA-RNA Assembly In Vivo. *ACS Synth. Biol.*, **6**, 1710–1721.

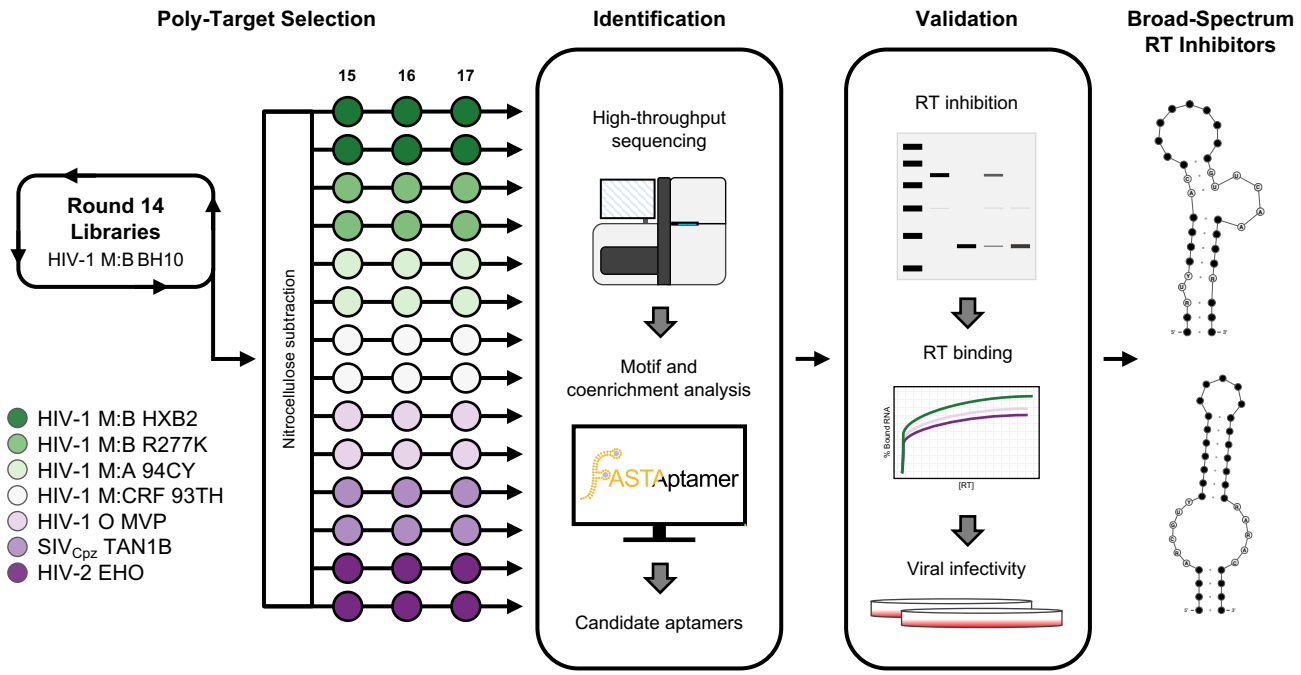

Figure 1. A Poly-Target selection strategy to identify broad-spectrum RT inhibitors. In the Poly-Target selection approach a pre-enriched aptamer library is subjected to additional rounds of systematic evolution of ligands by exponential enrichment (SELEX) against a panel of related targets along separate trajectories. In this work, 70N and 80N libraries that had been pre-enriched through 14 rounds of binding to an RT from HIV-1 M:B (BH10) (13) were first subjected to a negative selection (nitrocellulose subtraction) prior to three additional rounds of independent selections, in duplicate, against a panel of phylogenetically-distinct RTs from various strains of HIV-1, HIV-2 and SIV. Following the Poly-Target selection, high-throughput sequencing and coenrichment analysis were used to identify candidate broad-spectrum aptamers for downstream biochemical and biological validation.

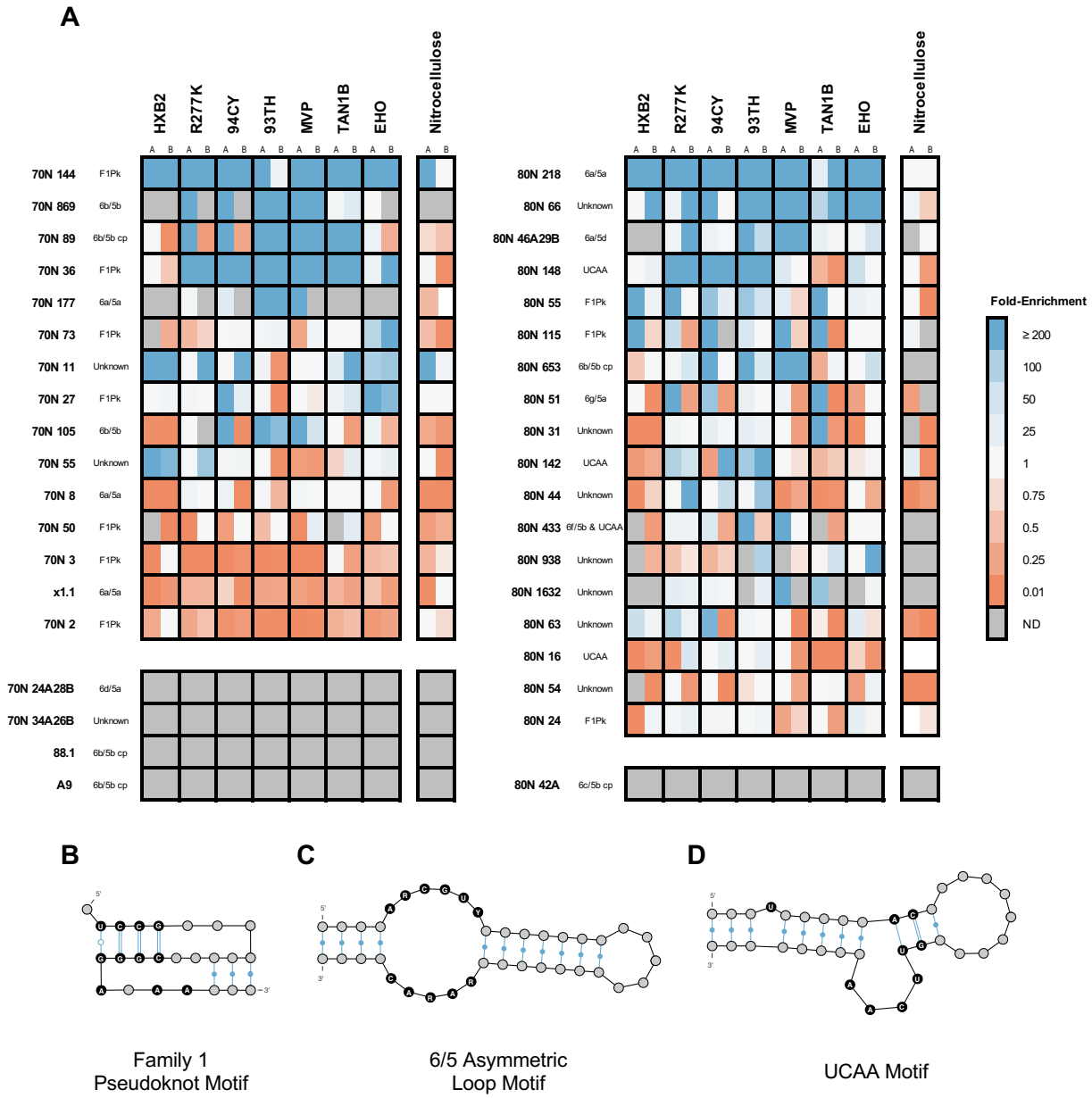

Figure 2. Coenrichment analysis identifies candidate broad-spectrum aptamers. (**A**) A heatmap of sequence fold-enrichment from the round 14 starting library of candidate aptamers depicts enrichment (blue) or depletion (orange) in each replicate selection trajectory (A or B) and in the nitrocellulose binding population. Aptamers are grouped by 70N (left set) or 80N (right set) and are sorted top-to-bottom by decreasing enrichment, averaged across all RT targets. Sequences included in the characterization but that were not detected (ND) in either round 14 or 17 and therefore did not have a enrichment value are colored in grey. Motif names are included to the right of the aptamer identity. Schematic depictions of the secondary structures of the major RT-inhibiting motifs: (**B**) Family 1 Pseudoknot (F1Pk), (**C**) 6/5 Asymmetric Loop ((6/5)AL) and (**D**) UCAA. Secondary structures generated using VARNA (58).

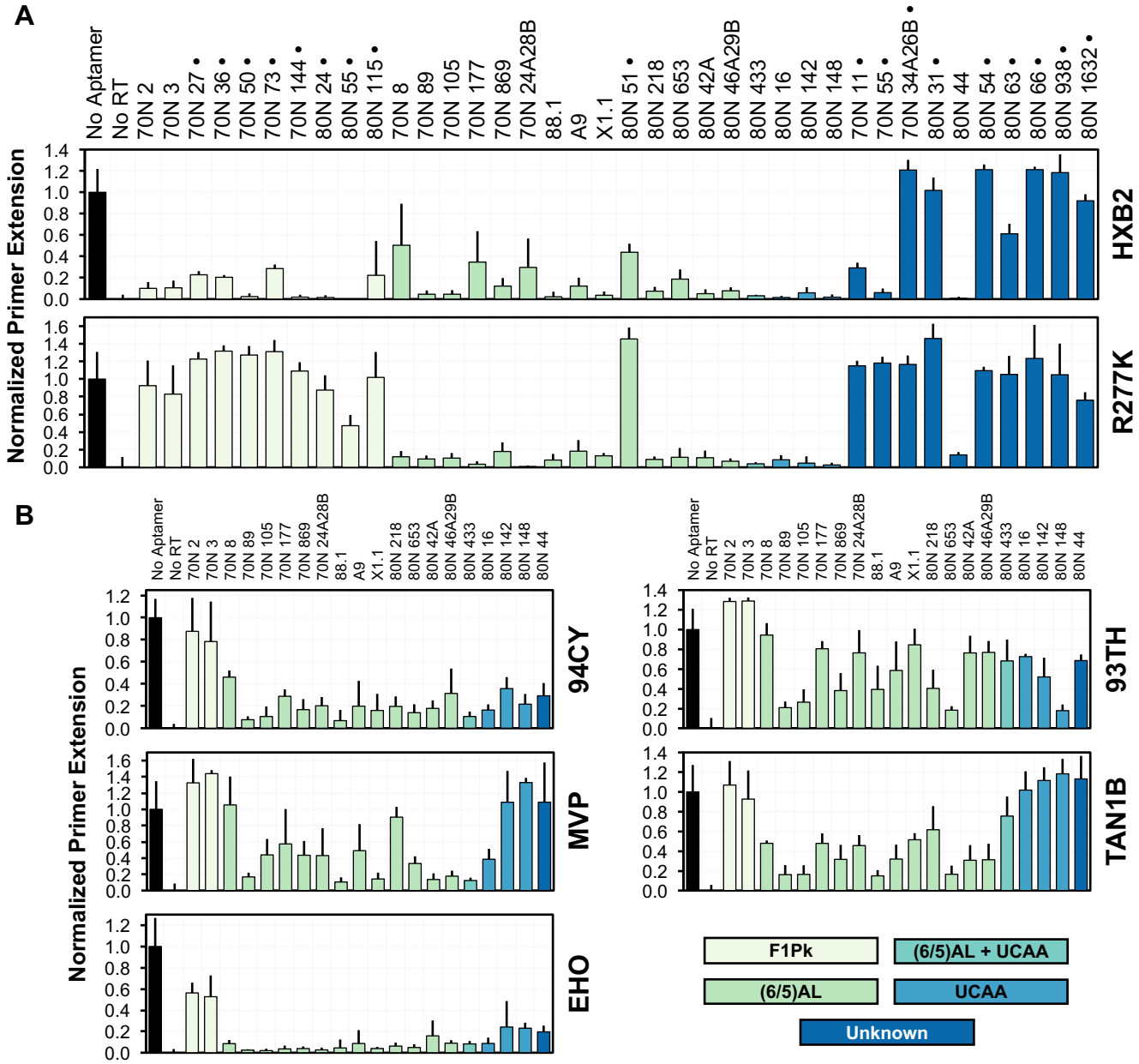

Figure 3. RT inhibition assays reveal broad-spectrum phenotypes. (**A**) Aptamer mediated inhibition of the DNA-dependent DNA polymerase activity of RT was determined through primer extension assays against HXB2 RT (top) and an R277K point mutant of HXB2 RT (bottom) for candidate aptamers identified through coenrichment analysis. Aptamers that failed to inhibit both RTs after two independent measurements (marked •) were eliminated from further examination, with the exception of 70N 2 and 70N 3. (**B**) Primer extension assays against non-Group M:B RTs in the selection panel reveal varying broad-spectrum inhibition. Columns are colored according to aptamer motif. Error bars indicate range for samples assayed in duplicate (marked •), whereas all other samples are n ≥ 5 and error bars indicate standard deviation.

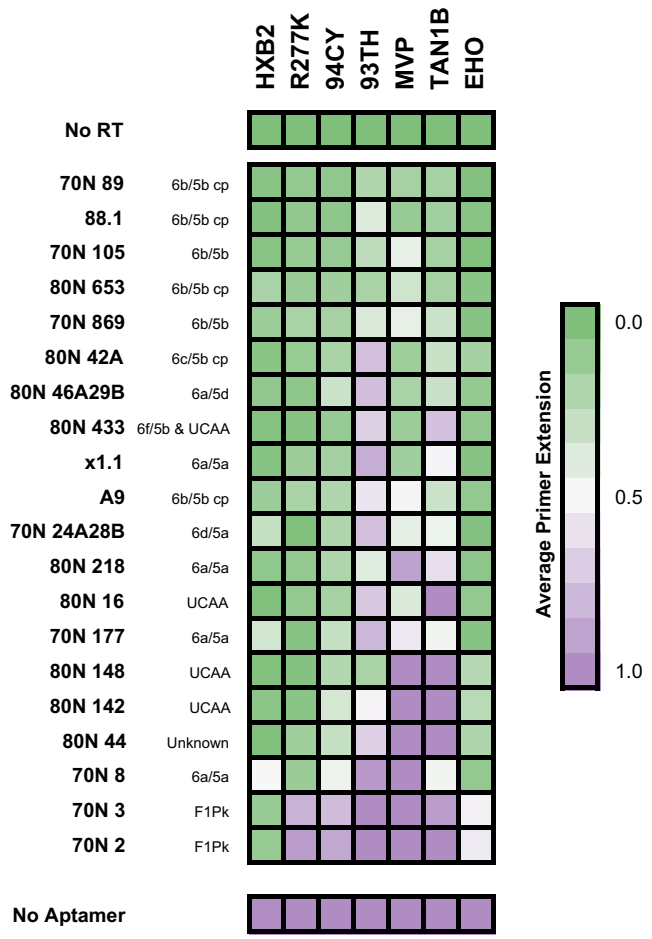

Figure 4. Inhibition profiles reveal motif-dependent broad-spectrum inhibition. Aptamers are sorted top-to-bottom by decreasing average inhibition, as measured by primer extension, against the panel of RTs used in the selection. Sorting in this manner reveals a pattern of biochemical RT inhibition corresponding to motif identity. (6/5)AL motifs, particularly the 6b/5b variant, demonstrated the strongest average inhibition against the tested RTs. UCAA motifs and the one previously-unidentified aptamer showed variable RT inhibition outside of Group M, and F1Pks showed no RT inhibition outside of Group M:B.

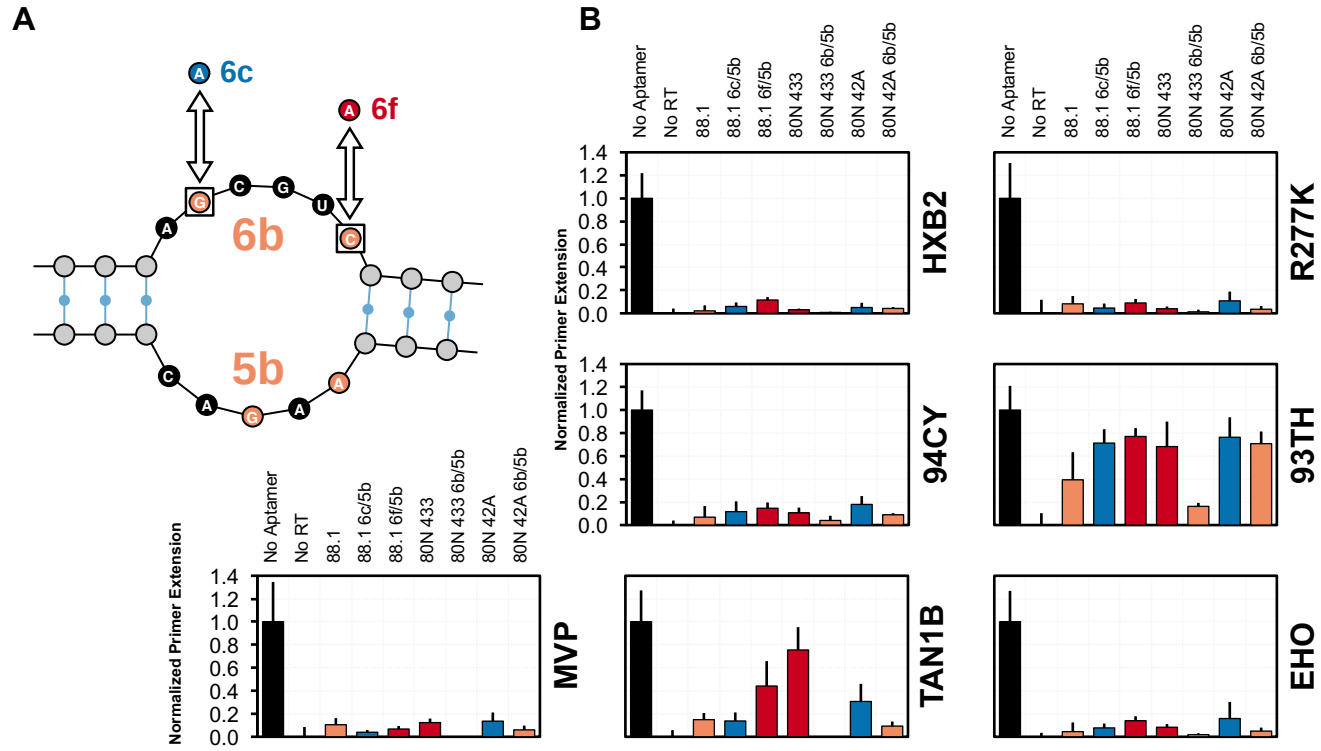

Figure 5. Conversion of exemplary (6/5)AL aptamers to the 6b/5b motif improves their broad-spectrum biochemical inhibition profile. (A) Single nucleotide conversions separate 6c/5b (blue) and 6f/5b (red) motifs from the 6b/5b motif (orange). Aptamer 88.1, which contains the 6b/5b motif, was converted to a 6f/5b or 6c/5b and assayed for changes in inhibition against RTs in the selection panel. Conversely, 80N 433 (a 6f/5b aptamer) and 80N 42A (a 6c/5b aptamer) were converted to 6b/5b. (**B**) Conversion towards the 6b/5b motif uniformly improved biochemical inhibition, whereas conversion away reduced inhibition in most cases. Mean values are shown (n ≥ 5) and error bars indicate standard deviation.

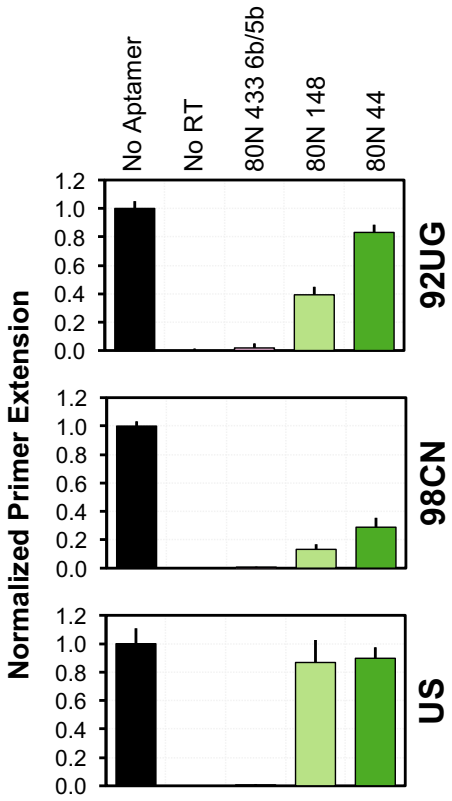

Figure 6. **Broad-spectrum aptamers are capable of RT inhibition outside of the selection panel.** Aptamers representing the three motifs with non-subtype B RT inhibition were tested against RTs from two group M strains (92UG and 98CN) and an SIV strain (US). 92UG, a circulating recombinant form of HIV-1 group M whose RT groups with subtype D, is inhibited moderately by the UCAA motif aptamer and robustly by the 6b/5b aptamer. RT from 98CN, a group M:C strain, is inhibited by all three aptamers tested, including 80N 44 (unknown motif). RT from the US strain of SIV_{CPZ}*Ptt*, is only inhibited by the 6b/5b aptamer. Mean values are shown (n ≥ 5) and error bars indicate standard deviation.

Table 1. Apparent binding affinity (K_d) of broad-spectrum RT aptamer-inhibitors[a]

	HXB2	R277K	94CY	93TH	MVP	TAN1B	EHO
70N 2	110 ± 20	>>300	-	-	-	-	-
80N 44	60 ± 12	190 ± 51	30 ± 9	58 ± 17	-	-	-
80N 148	74 ± 17	150 ± 42	55 ± 13	13 ± 3	-	-	-
80N 433	59 ± 23	-	-	22 ± 6	-	210 ± 38	-
80N 433bb	22 ± 4	38 ± 7	29 ± 8	7 ± 1	39 ± 8	16 ± 2	34 ± 9

[a]Values are listed in nanomolar with standard deviation from triplicate assays.
Binding curves are provided in Supplementary Figure S17.

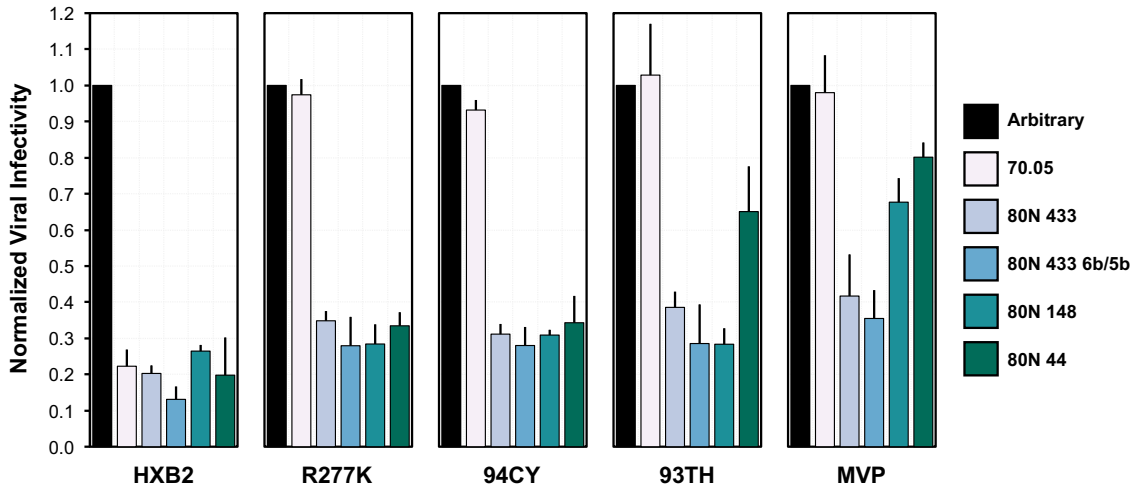

Figure 7. Broad-spectrum anti-RT aptamers suppress viral replication in biological assays. A non-inhibitory RNA ("arbitrary"), a previously characterized F1Pk aptamer (70.05), and several broad-spectrum aptamers identified through Poly-Target selection were assessed for their ability to suppress virus in a single-cycle infectivity assay.

Supplementary Data

Poly-Target Selection Identifies RNA Broad-Spectrum Inhibitors of HIV Reverse Transcriptases

Khalid K. Alam[1,2,5], Jonathan L. Chang[2,3], Margaret J. Lange[2,3], Phuong D.M. Nguyen[1,2], Andrew W. Sawyer[1,2], & Donald H. Burke[1,2,3,4,*]

[1]Department of Biochemistry, [2]Bond Life Sciences Center, [3]Department of Molecular Microbiology and Immunology, [4]Department of Biological Engineering, University of Missouri, Columbia, MO, USA

[5]Current address: Department of Chemical and Biological Engineering, Northwestern University, Evanston, IL, USA

*Corresponding author: burkedh@missouri.edu

Supplementary Figure S1 28
Supplementary Table S1 29
Supplementary Figure S2 30
Supplementary Table S2 31
Supplementary Figure S3 32
Supplementary Figure S4 33
Supplementary Figure S5 34
Supplementary Figure S6 35
Supplementary Figure S7 36
Supplementary Figure S8 37
Supplementary Table S3 38
Supplementary Table S4 39
Supplementary Figure S9 40
Supplementary Figure S10 41
Supplementary Table S5 42
Supplementary Figure S11 43
Supplementary Figure S12 44
Supplementary Figure S13 45
Supplementary Figure S14 46
Supplementary Figure S15 47
Supplementary Figure S16 48
Supplementary Figure S17 49
Supplementary Table S6 50

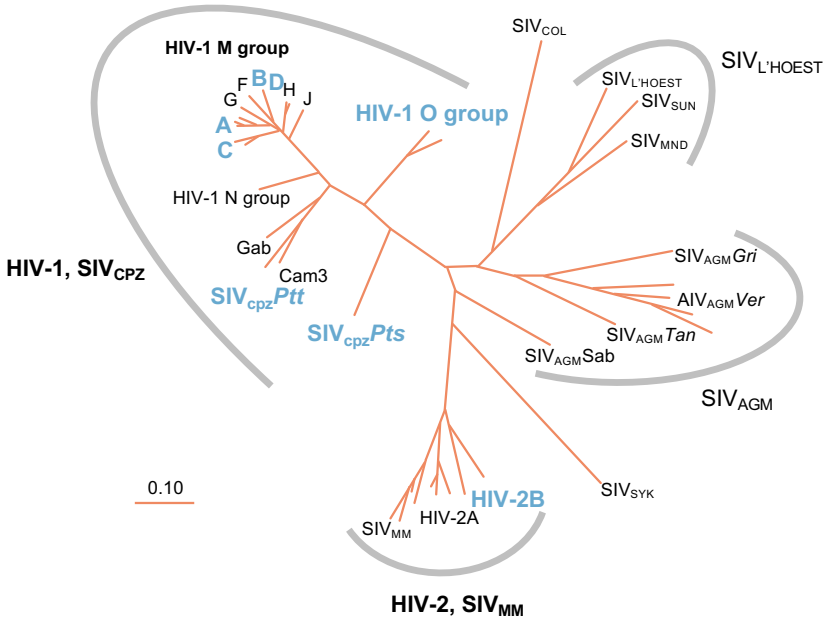

Figure S1 Phylogenetic relationships among the primate lentivirus *Pol* gene.

The lentiviral *Pol* gene codes for reverse transcriptase, protease, RNase, and integrase. Relative to the rest of the viral genome, *Pol* is highly conserved and is therefore used to construct phylogenetic relationships among lentiviral strains. The phylogenetic tree depicted here illustrates the genetic diversity both within and across lentiviral groups. Reverse transcriptase from the groups and subtypes used in this study are shown in bold and colored blue. Adapted, with permission, from The Human Retroviruses and AIDS 1999 Compendium (https://www.hiv.lanl.gov/).

Table S1 Panel of recombinant RTs used in Poly-Target selection and characterization.

Virus (Group:Subtype)	Strain[a]	GenBank Accession Number	Differences from Reference Sequence
HIV-1 (M:B)	**HXB2**	K03455	-
HIV-1 (M:B)	HXB2 (**R277K**)	K03455	R277K[b]
HIV-1 (M:A)	**94CY**017.41	AF286237	S554T
HIV-1 (M:CRF01_AE)	**93TH**253.3	U51189	D6E, I553S, S554T
HIV-1 (O)	**MVP**5180	L20571	M16V, I184M, V261I, V435I, N465K, E523K
SIV_{Cpz}*Pts*	**TAN1B**	AF447763	-
HIV-2 (B)	**EHO**	U27200	E15G, K64R, K66R, N176S, K206R, A449V, E520K
HIV-1 (M:A/D)[c]	**92UG**021	AF009396	D121C, E169D, V293I
HIV-1 (M:C)[c]	**98CN**009	AF286230	R102K, S554T
SIV_{Cpz}*Ptt*[c]	**US**	AF103818	Y208H, E223K, H315R, R345Q, L392P, G498D, V518A

[a]Abbreviated names (in bold) are used throughout document to refer to the strains listed here.
[b]R277K mutation only present in p66 subunit.
[c]Reverse transcriptases not included the selection panel, but used to characterize broad-spectrum inhibition.

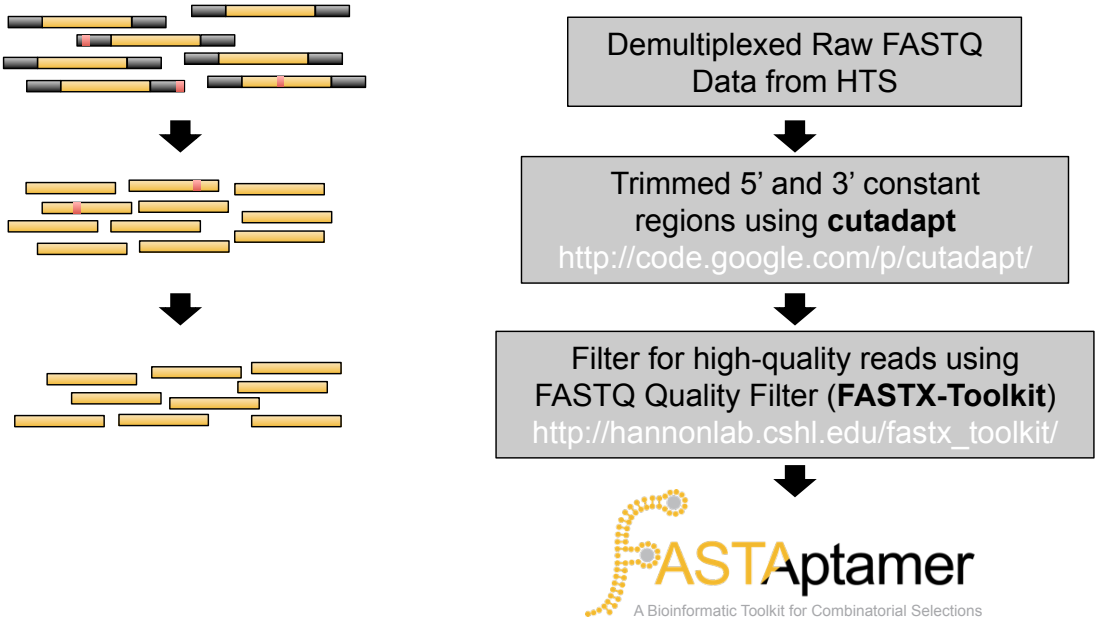

Figure S2 Pre-processing workflow for sequencing of Poly-Target selection populations.

High-throughput sequencing populations were pre-processed to isolate only high-quality reads of the randomized regions. Raw FASTQ files were demultiplexed into individual populations using custom Perl scripts. Constant regions (represented by the black bars) were then removed using cutadapt (57). Trimmed reads were filtered using FASTQ Quality Filter from the FASTX-Toolkit (http://hannonlab.cshl.edu/fastx_toolkit/) to remove sequences that contained any nucleotides called with < 99% confidence (red bars). Trimmed and filtered files were then processed using the FASTAptamer toolkit to determine sequence frequencies, compare selection populations, calculate fold-enrichment from the Round 14 starting libraries, group related sequences into clusters and search for sequence motifs (33).

Table S2 Read counts (total, unique, reads per sequence) and number of unique sequence clusters from high throughput sequencing of Poly-Target populations.

Library ID	Total Reads	Unique Reads	Average Reads / Sequence[a]	Sequence Clusters
70N Round 14	2,160,216	72,921	30	1,250
70N Nitrocellulose (A)	2,511,963	91,959	27	920
70N Nitrocellulose (B)	2,899,030	69,245	42	283
70N HXB2 (A)	3,684,892	61,680	60	218
70N HXB2 (B)	4,870,444	66,853	73	186
70N R277K (A)	3,020,692	68,982	44	300
70N R277K (B)	1,887,624	45,672	41	79
70N 94CY (A)	6,738,111	108,429	46	440
70N 94CY (B)	3,461,804	75,532	40	251
70N 93TH (A)	3,396,938	85,129	53	381
70N 93TH (B)	2,890,287	54,963	45	223
70N MVP (A)	2,978,909	65,695	48	377
70N MVP (B)	2,705,454	56,625	22	152
70N TAN1B (A)	786,244	36,365	37	210
70N TAN1B (B)	3,812,018	102,433	34	431
70N EHO (A)	1,218,522	35,474	51	236
70N EHO (B)	3,630,580	71,575	30	327
80N Round 14	5,867,479	555,340	11	2,493[b]
80N Nitrocellulose (A)	6,690,767	264,381	25	645
80N Nitrocellulose (B)	3,419,851	141,948	24	248
80N HXB2 (A)	1,699,288	64,646	26	376
80N HXB2 (B)	3,837,366	90,029	43	448
80N R277K (A)	2,808,546	155,071	18	2,069
80N R277K (B)	3,590,015	131,326	27	751
80N 94CY (A)	3,509,589	141,320	25	1,745
80N 94CY (B)	2,268,560	90,148	25	941
80N 93TH (A)	1,638,888	29,631	55	698
80N 93TH (B)	2,195,494	113,588	19	4,870
80N MVP (A)	2,419,317	96,535	25	892
80N MVP (B)	3,602,286	148,951	24	1,103
80N TAN1B (A)	3,029,430	156,918	19	3,470
80N TAN1B (B)	2,761,963	88,458	31	344
80N EHO (A)	2,228,795	80,630	28	658
80N EHO (B)	2,687,668	109,327	25	2,720

[a]Rounded to nearest whole number.
[b]To reduce computational load, cluster generation for 80N Round 14 population was performed only on sequences sampled more than once (107,951 unique sequences).

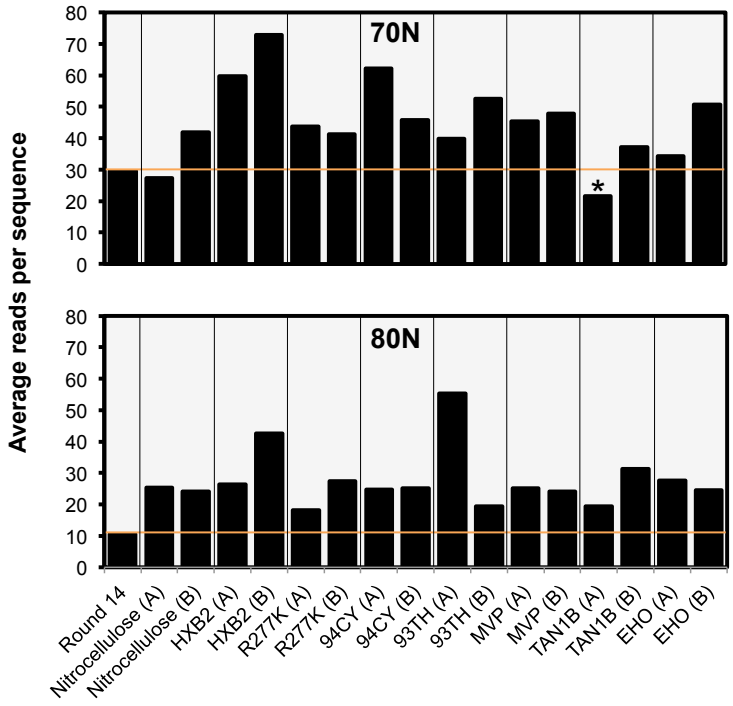

Figure S3 Enrichment of Poly-Target selection trajectories.

The average reads per sequence of an aptamer library can be used to monitor the convergence of sequence space of a population when compared to a preceding population. Enrichment was observed in all of the 70N (top) and 80N (bottom) round 17 Poly-Target populations sampled with greater than 1 million reads. A single library, 70N round 17 TAN1B (A), marked with the asterisk had low sampling depth (786,244 reads) and may underrepresent the true diversity of the library relative to the round 14 populations. Orange bars indicate the average reads per sequence of the starting populations for Poly-Target selection.

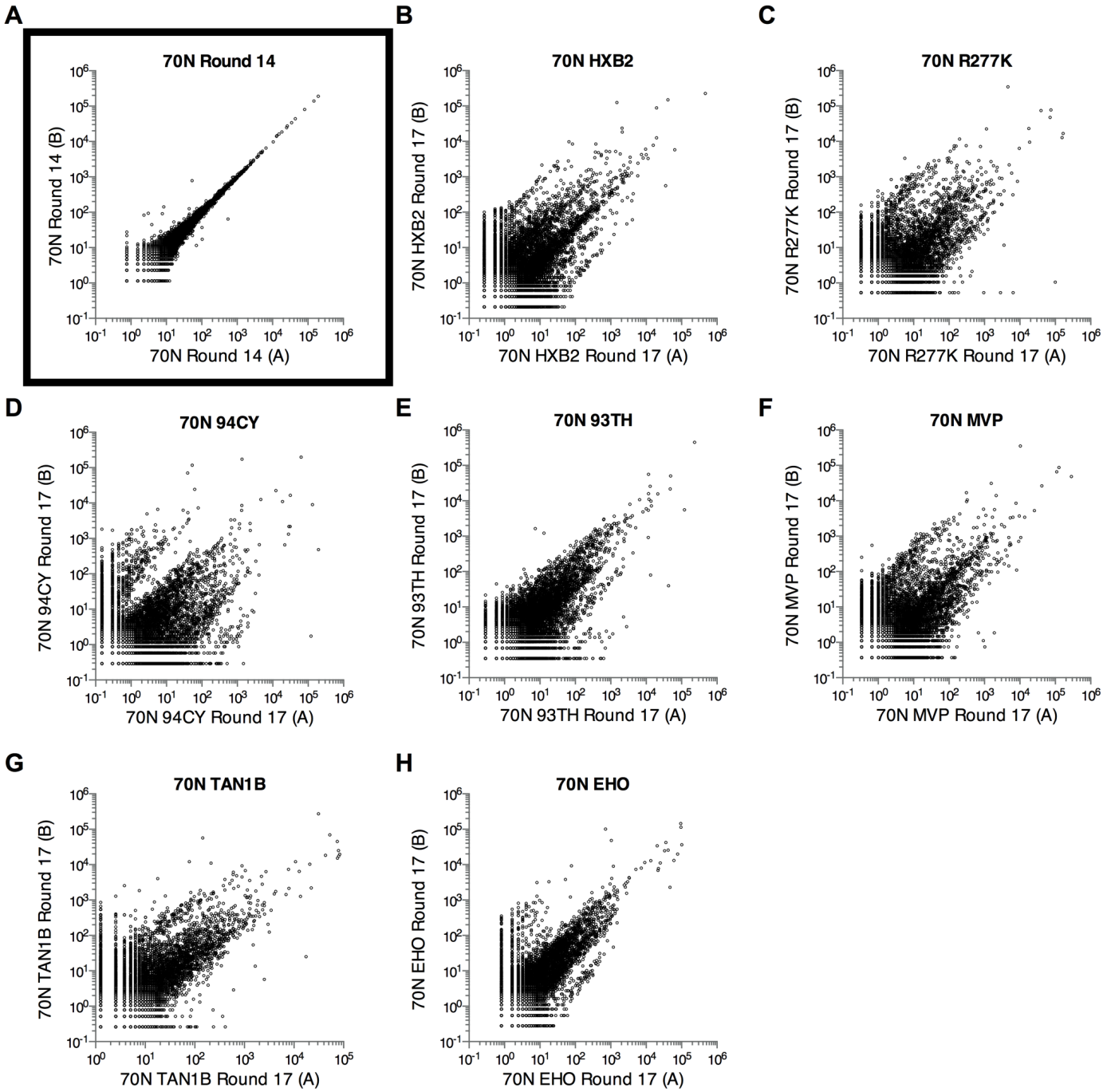

Figure S4 Comparison of 70N replicate trajectories.

Comparison of sequence read frequencies in replicate sampling of the 70N round 14 library (**A**), and of replicate selection trajectories after three rounds. (**B**) 70N HXB2 round 17, (**C**) 70N round 17 R277K, (**D**) 70N round 17 94CY, (**E**) 70N round 17 93TH, (**F**) 70N round 17 MVP, (**G**) 70N round 17 TAN1B, (**H**) 70N round 17 EHO. Units of *x*- and *y*-axes are in reads per million and plotted on a logarithmic scale. Sequences sampled only once are not shown.

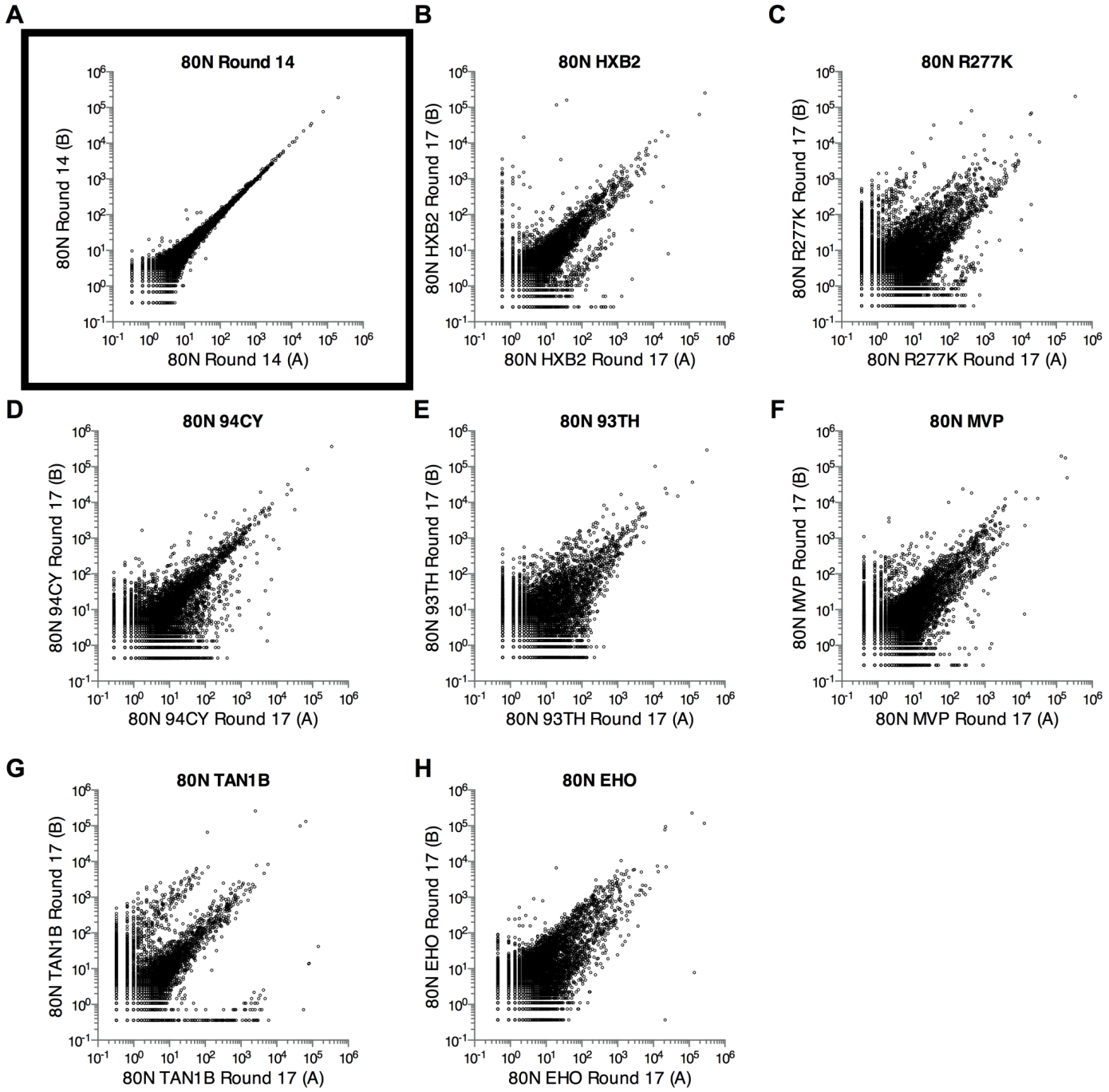

Figure S5 Comparison of 80N replicate trajectories**.**

Comparison of sequence read frequencies in replicate sampling of the 80N round 14 library (**A**), and of replicate selection trajectories after three rounds. (**B**) 80N HXB2 round 17, (**C**) 80N round 17 R277K, (**D**) 80N round 17 94CY, (**E**) 80N round 17 93TH, (**F**) 80N round 17 MVP, (**G**) 80N round 17 TAN1B, (**H**) 80N round 17 EHO. Units of *x*- and *y*-axes are in reads per million and plotted on a logarithmic scale. Sequences sampled only once are not shown.

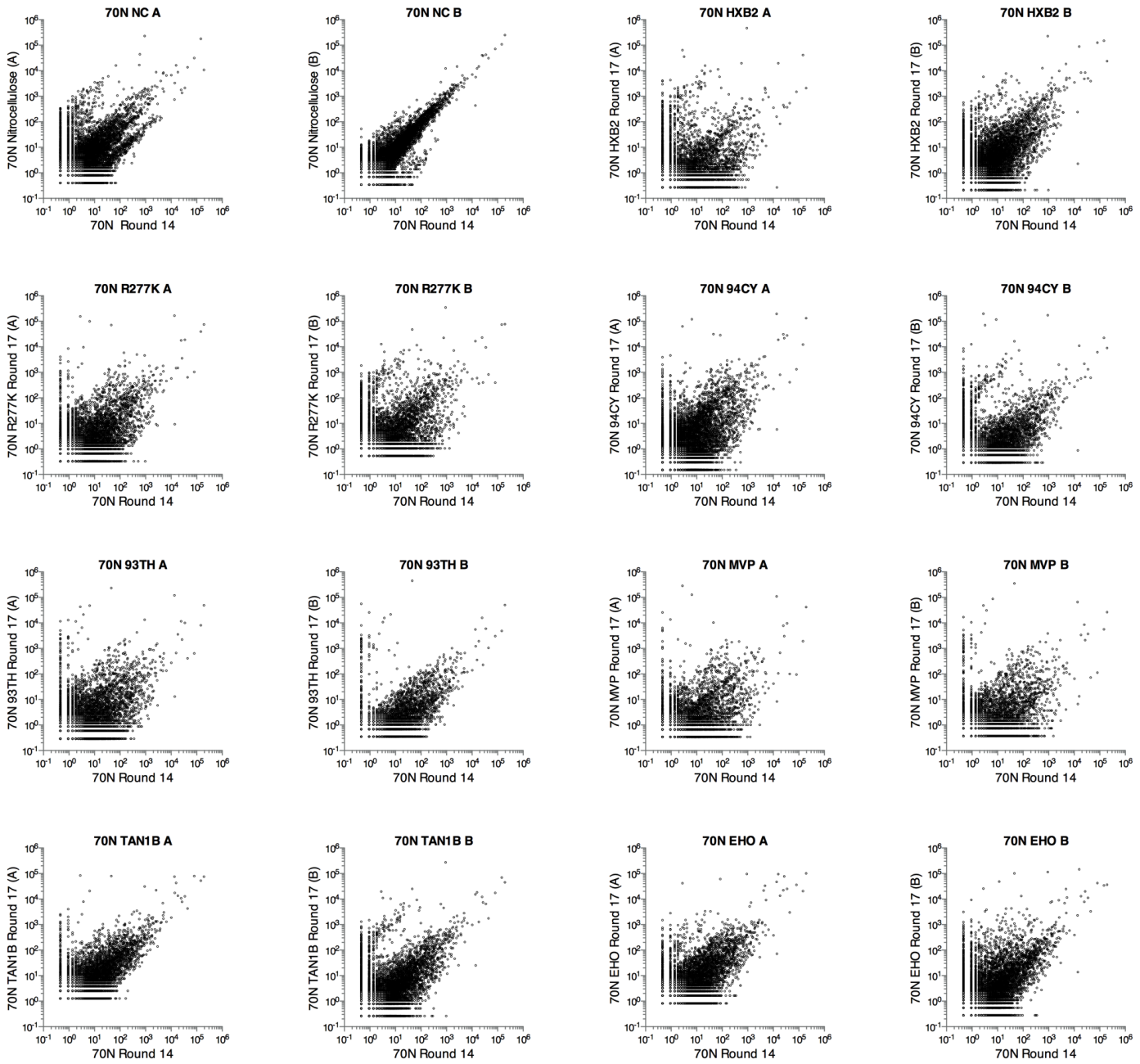

Figure S6 Comparison of 70N round 17 trajectories with the starting round 14 libraries.

Comparison of sequence frequencies in 70N round 14 versus nitrocellulose binding population replicates, HXB2 replicates, R277K replicates, 94CY replicates, 93TH replicates, MVP replicates, TAN1B replicates and EHO replicates. Units of *x*- and *y*-axes are in reads per million and plotted on a logarithmic scale. Sequences sampled only once are not shown.

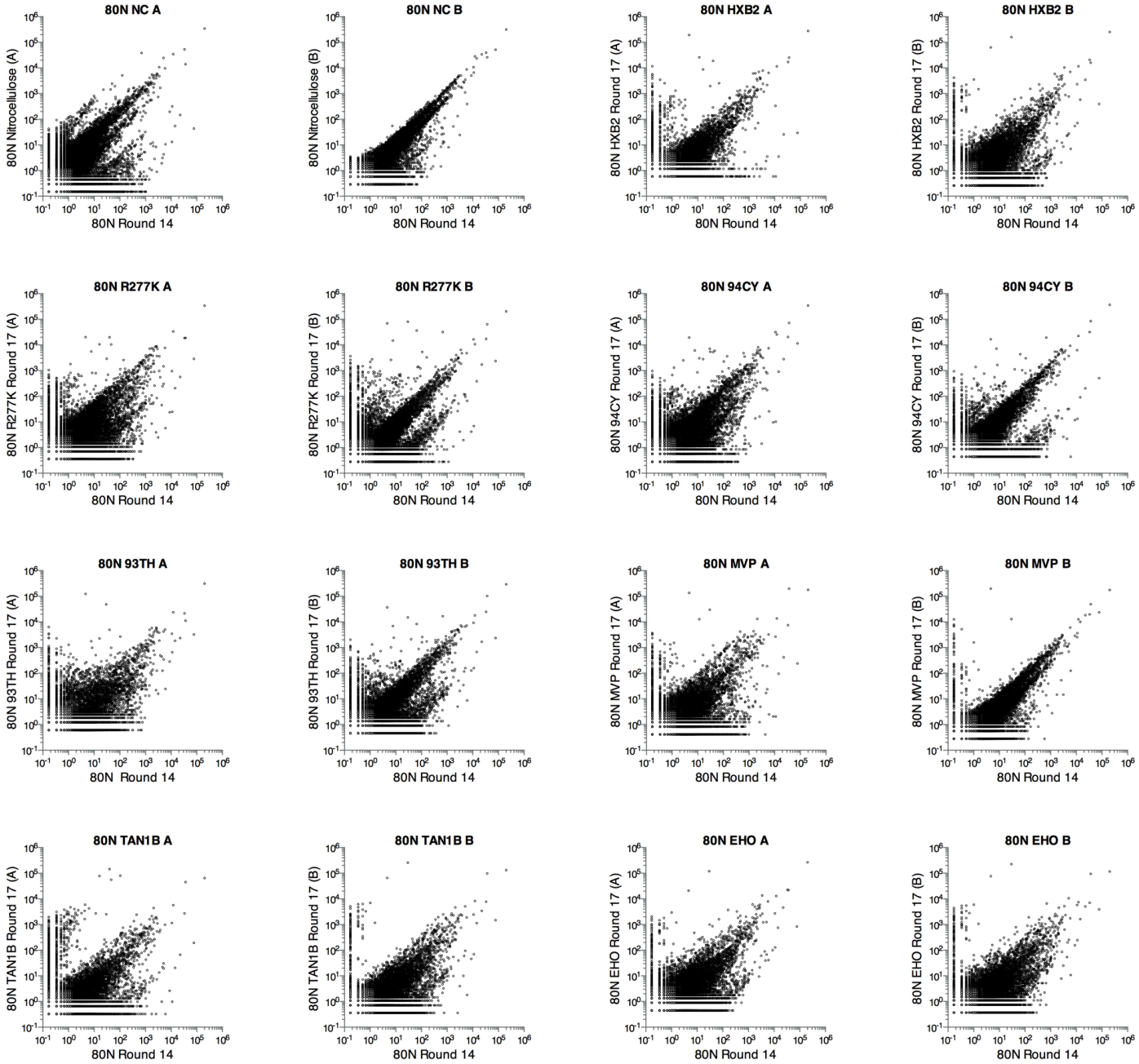

Figure S7 Comparison of 80N round 17 trajectories with the starting round 14 libraries.

Comparison of sequence frequencies in 80N round 14 versus nitrocellulose binding population replicates, HXB2 replicates, R277K replicates, 94CY replicates, 93TH replicates, MVP replicates, TAN1B replicates and EHO replicates. Units of *x*- and *y*-axes are in reads per million and plotted on a logarithmic scale. Sequences sampled only once are not shown.

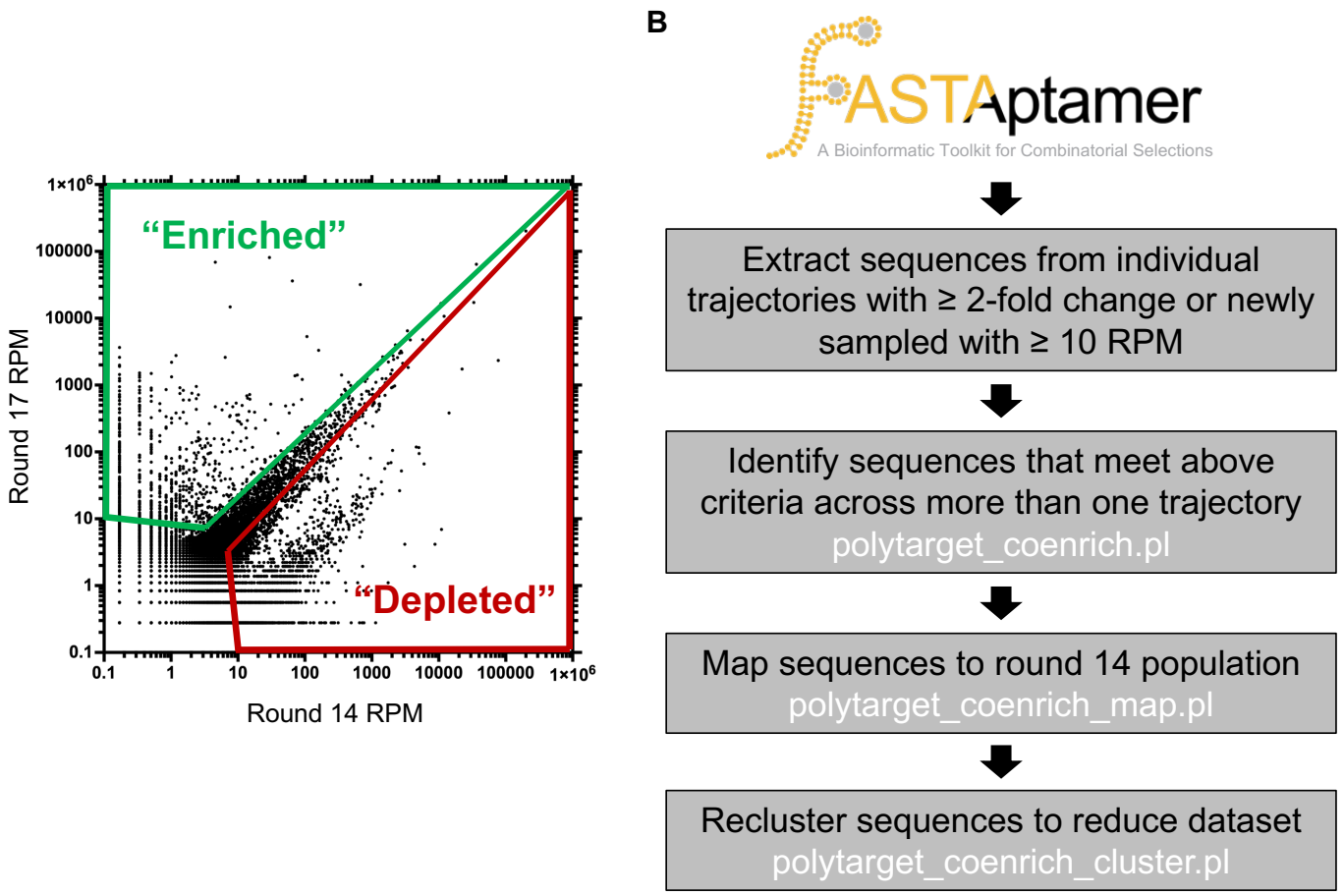

Figure S8 Enrichment and depletion criteria for inclusion into coenrichment analysis.

Sequences with at least 10 reads per million (RPM) in aggregate (round 14 RPM + round 17 RPM) were considered in coenrichment analysis. We defined enrichment as ≥ 2-fold increase in sequence RPM (green) and depletion as ≥ 2-fold decrease in sequence RPM from round 14 to round 17 (red). Also included were sequences that were only present at ≥10 RPM in either round 14 (depletion) or round 17 (enrichment) alone, which are not plotted on the graph. (**A**) Shown here is a representative diagram of sequences that would meet the criteria in a single selection trajectory. (**B**) The bioinformatic pipeline for coenrichment analysis began by parsing FASTAptamer-Enrich files for sequences that meet the enrichment or depletion criteria in an individual trajectory (33). Those sequences are then compared across trajectories to identify coenrichers/codepleters, mapped to their round 14 identity (if available), and reclustered to focus characterization on the most represented sequence within a cluster. Perl scripts used for coenrichment analysis are freely available at https://github.com/FASTAptamer/PolyTarget.

Table S3 Number of sequences considered enriched or depleted in each Poly-Target selection trajectory.

Library ID	Enriched Sequences[a]	Depleted Sequences[b]
70N Nitrocellulose (A)	1,862	1,948
70N Nitrocellulose (B)	475	808
70N HXB2 (A)	1,660	2,652
70N HXB2 (B)	1,121	2,130
70N R277K (A)	1,742	2,458
70N R277K (B)	1,579	2,365
70N 94CY (A)	1,487	2,174
70N 94CY (B)	1,921	1,615
70N 93TH (A)	2,297	2,470
70N 93TH (B)	1,671	2,686
70N MVP (A)	2,019	2,585
70N MVP (B)	1,731	2,590
70N TAN1B (A)	1,861	1,832
70N TAN1B (B)	1,889	2,415
70N EHO (A)	1,454	1,955
70N EHO (B)	1,679	2,291
80N Nitrocellulose (A)	2,485	2,773
80N Nitrocellulose (B)	430	1,498
80N HXB2 (A)	1,793	3,496
80N HXB2 (B)	1,330	3,620
80N R277K (A)	2,880	3,097
80N R277K (B)	1,826	3,052
80N 94CY (A)	1,964	2,916
80N 94CY (B)	1,691	2,600
80N 93TH (A)	2,736	3,494
80N 93TH (B)	1,969	2,614
80N MVP (A)	2,002	3,382
80N MVP (B)	1,321	2,979
80N TAN1B (A)	2,901	3,706
80N TAN1B (B)	1,704	3,532
80N EHO (A)	1,496	3,397
80N EHO (B)	1,887	3,439

[a]Enriched sequences are defined as those with a minimum of 10 reads per million (RPM) that either experienced at least 2-fold enrichment from the round 14 library, or that were not present in round 14 but appeared in round 17.
[b]Depleted sequences are defined as those with a minimum of 10 reads per million (RPM) that either experienced 2-fold depletion or more (≤ 0.5-fold enrichment) from the round 14 library, or that were no longer sampled in round 17.

Table S4 Number of sequences that coenriched or codepleted across Poly-Target selection trajectories.

Library	Coenriched Sequences[a]	Codepleted Sequences[b]
70N (A)	2,129 [3,170]	1,095 [2,971]
70N (B)	2,524 [2,778]	2,222 [2,953]
80N (A)	2,575 [3,798]	1,429 [4,145]
80N (B)	2,823 [2,959]	2,604 [4,015]

[a]Coenriched sequences are defined as those that met our criteria for enrichment in at least 2 selection trajectories.
[b]Codepleted sequences are defined as those that met our criteria for depletion in at least 2 selection trajectories.
Values in brackets refer to the number of sequences that coenriched or codepleted in 2 trajectories prior to subtraction of the nitrocellulose population.

	70N Rd. 14 Cluster ID	70N (A)				70N (B)			
		Coenrich Cluster ID	Unique Sequences	Codeplete Cluster ID	Unique Sequences	Coenrich Cluster ID	Unique Sequences	Codeplete Cluster ID	Unique Sequences
	1	1	89	1	44	1	75	1	749
•	2			2	660	2	25	2	679
•	3	2	6	3	111	3	21	3	270
	4	3	15	4	5	4	2	4	208
	5	4	2	5	69			5	157
	6	5	107	6	124	5	258	6	84
	7			7	2			7	15
•	8	6	350	8	1	6	38	8	3
	9			9	35			9	38
	10			10	6	7	5	10	1
•	11	7	13	11	1	8	498		
	12							11	3
	13			12	5	9	2	12	5
	14			13	3			13	2
	17			14	3				
	20							14	1
	21			15	1				
	24			16	2	10	11	15	2
	26			17	2				
•	27	8	107			11	31		
	28			18	1	12	12		
	30			19	1			16	1
	31			20	1				
	32			21	1	13	4	17	1
	33			22	1				
•	36	9	430			14	769		
	38			23	1				
	39			24	2				
	43			25	1				
	44			26	1				
•	50					15	4		
	52			27	3	16	44	18	1
	53			28	1				
•	55	10	3			17	24		
	56			29	1				
	57			30	1				
	58			31	1				
	61			32	1			19	1
	64			33	1				
•	73	11	1			18	1		
	75			34	1				
	82			35	1	19	5	20	1
•	89	12	272			20	94		
•	105	13	11			21	2		
	112	14	2						
	134					22	88		
•	144	15	412			23	185		
	157	16	1			24	1		
	158	17	3						
	168	18	2						
•	177	19	22						
	263	20	2						
	445	21	1						
•	869	22	53			25	19		
		23	1						
•		24	179			28	27		
		25	2						
		26	1						
		27	63			27	4		
		28	2						
		29	2						
		30	1						
		31	7			30	1		
		32	29						
		33	2			29	1		
•		34	3			26	273		
		35	2						
		36	1						

	80N Rd. 14 Cluster ID	80N (A)				80N (B)			
		Coenrich Cluster ID	Unique Sequences	Codeplete Cluster ID	Unique Sequences	Coenrich Cluster ID	Unique Sequences	Codeplete Cluster ID	Unique Sequences
	1	1	155	1	987	1	189	1	1047
	2			2	30			2	435
	3	2	270	3	118	2	429	3	64
	4			4	15			4	529
	5							5	261
	6	3	16	5	12	3	1	6	167
	8			6	107	4	4	7	2
	9							8	47
	10	4	11	7	94	5	119	9	27
	11			8	1				
	12			9	1	6	1	10	2
	13	5	37	10	9			11	3
	14							12	2
	15			11	13	7	38	13	1
•	16	6	36	12	1	8	163	14	2
	17			13	1			15	2
	18	7	40	14	2			16	3
	19	8	1	15	11			17	1
	21			16	11				
	23			17	1				
•	24	9	54			9	59	18	2
	25			18	3				
	26	10	55			10	3	19	1
•	31	11	66			11	9		
	35	12	40	19	2	12	6		
	41	13	3			13	3		
	43			20	1				
•	44	14	2			14	141		
•	51	15	157						
•	54	16	8	21	1	15	21		
•	55	17	391			16	31		
	60	18	6			17	7	20	2
•	63	19	49			18	5		
•	66	20	198			19	867		
	70	21	2						
	76	22	3						
	96			22	1				
•	115	23	162			20	1		
	126			23	1				
	130	24	2	24	1			21	1
	135			25	1				
	136							22	1
	137			26	1			23	1
	139			27	1			24	1
	141			28	1				
•	142	25	5	29	1	21	30		
•	148	26	105			22	154		
	178	27	1						
•	218	28	628			23	523		
	259	29	2						
	279	30	2						
	302	31	6			24	1		
	325	32	1						
	406	33	1						
•	433	34	9						
	446	35	2						
	579	36	3						
•	653	37	4			25	1		
•	938					26	2		
•	1632	38	2						
	1839	39	1						
	2076	40	2						
		41	13						
•		42	8						
		43	4						
		44	1			27	8		
		45	1			28	1		
•		46	4			29	4		
		47	6			30	1		
						31	1		

Figure S9 Coenrichment and codepletion analysis of clusters reveal the emergence of rare sequence clusters.

Within each replicate trajectory, clusters of related sequences that experienced only depletion are highlighted in gold and those that experienced only enrichment are highlighted in purple. Clusters containing sequences that both enriched and depleted are highlighted in gray. Cluster identities in round 17 populations are traced back to and named after their original cluster identity in the round 14 libraries for comparison within the 70N or 80N subsets. Abundant clusters with large numbers of closely-related sequences include individual cluster members that score as co-enriching and others that score as co-depleting, such that the cluster as a whole is subject to both depletion and enrichment. Clusters that were rare in round 14 almost exclusively experienced enrichment. Dots (•) to the left of cluster designations indicate clusters that were chosen for further analysis.

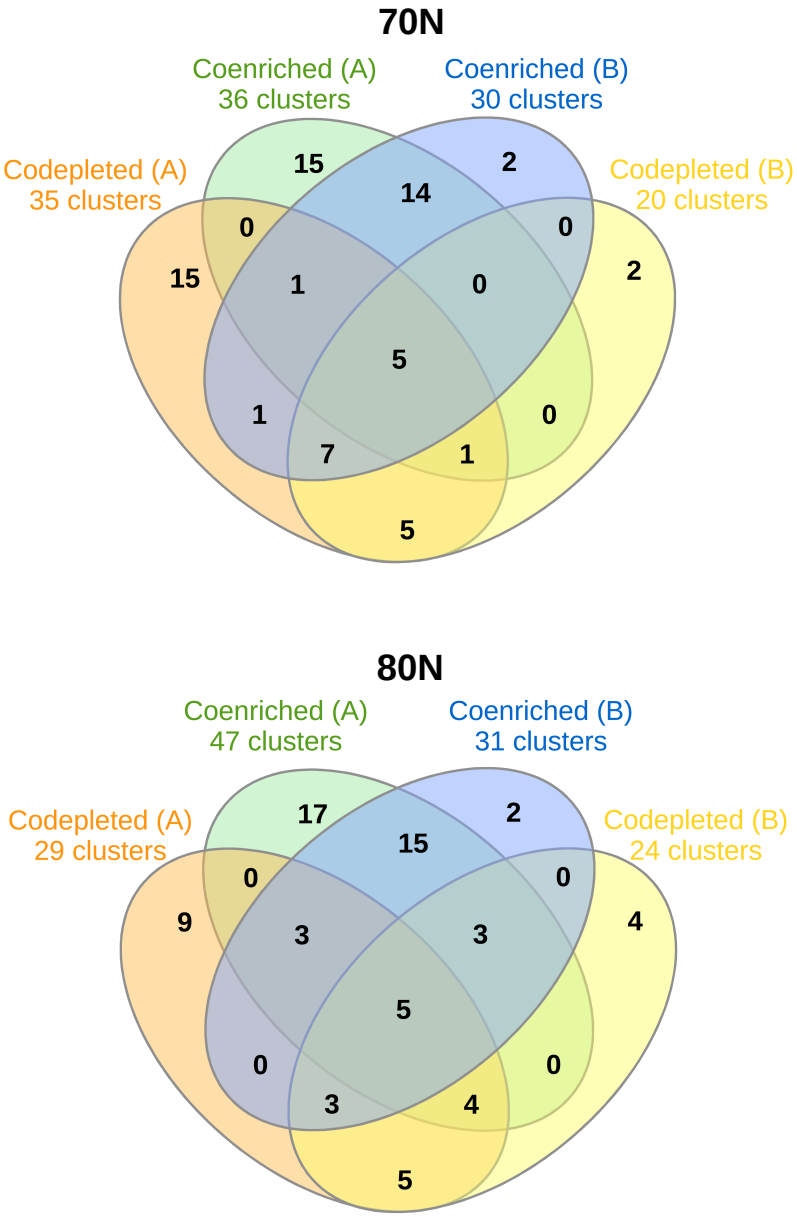

Figure S10 Set diagram of coenriched and codepleted clusters from the 70N and 80N selections.

Selection of candidate aptamers was informed by the identification of clusters that experienced coenrichment and/or codepletion from the 70N (top) and 80N (bottom) libraries. Of particular interest were the clusters that experienced only coenrichment in either or both of the replicates.

Table S5 Reads per million of candidate aptamers identified through Poly-Target selection and coenrichment/cordepletion analysis.

Aptamer	Round 14	Nitrocellulose		HXB2		R277K		94CY		93TH		MVP		TAN1B		EHO	
		A	B	A	B	A	B	A	B	A	B	A	B	A	B	A	B
88.1						15.89		122.29		90.38	2.77	853.33	278.33	2.54	3.15		0.28
A9		0.40		0.27		6,458.45	0.53	369.54		52.99		1,027.22	0.74	57.23	6.56		0.55
x1.1	193,358.44	10,754.14	249,949.47	2,078.22	23,689.63	75,460.52	77,868.79	132,206.79	9,019.00	48,784.23	50,265.94	41,563.54	26,432.53	74,882.61	45,041.76	100,861.54	36,708.18
70N 2	145,037.35	177,233.90	108,754.65	40,913.82	149,959.84	39,625.03	74,346.37	12,357.91	22,571.47	8,072.56	4,885.67	1,916.47	5,610.52	52,643.96	69,970.29	20,511.73	34,147.99
70N 3	80,591.14	31,459.46	71,254.52	1,468.88	126,060.38	1,033.54	393.09	1,319.51	6,163.26	642.64	3,050.91	95.67	113.10	79,678.83	17,487.33	36,115.88	42,435.92
70N 8	13,453.28	739.26	432.90	158.76	239.81	166,827.01	16,777.71	194,427.79	479.81	121,129.68	5,543.05	109,306.13	65,905.76	75,217.11	15,213.20	46,776.34	2,295.23
70N 11	914.26	229,777.27	12,217.88	465,857.07	227,577.61	4,617.49	347,901.91	1,363.14	172,936.13	13,402.07	79.58	1,091.34	3,867.74	31,196.42	275,150.85	95,765.20	114,451.96
70N 27	83.79	198.65	132.46	211.40	779.81	650.18	283.95	28,741.29	2,181.81	750.09	2.08	192.69	73.19	1,271.87	3,555.60	60,660.37	13,216.35
70N 36	45.37	406.06	2.76	137.32	26.08	71,328.36	47,764.28	31,382.24	16,615.04	233,971.89	447,829.23	10,356.14	355,491.17	79,148.46	25,084.35	714.80	101,233.41
70N 50	22.68	3.98	7.59		0.41	0.33	68.87	4.01	54.31	10.30	66.43	0.67	552.59		661.59	4.10	68.03
70N 55	20.37	37.42	1.03	8,185.59	3,389.01	116.86	2,561.95	144.40	227.34	107.16	1.38	3.69	2.96	13.99	552.46	128.84	481.19
70N 73	11.57	5.57	0.69		3.70	4.97	7.95	56.40	73.66	93.02	160.88	3.02	107.93	26.71	65.58	1,031.58	48,583.97
70N 89	6.48	4.78	3.45	7.87	0.41	99,429.53	1.06	120,145.99	1.73	47,644.67	21,649.75	127,350.32	87,576.06	20,826.87	10,366.16	115.71	2.20
70N 105	5.56	1.59	0.69	0.27	0.21	10.59		1,499.83	0.29	2,355.06	845.24	1,316.25	290.52	13.99	1.05	82.89	2.20
70N 144	2.78	1,154.48	9.66	64,021.14	5,819.18	154,992.63	12,860.61	63,228.85	196,921.89	42,754.68	39.79	284,496.10	48,078.81	83,959.94	19,780.86	41,858.91	25,797.26
70N 177	1.85	0.80				15.23		62.33		11,484.46	921.36	2,260.89					
70N 869	0.46					240.01		2,004.42		5,096.65	1,736.16	25,866.52	5,271.57	3.82	16.00	0.82	
70N 24A28B						16.88	0.53	74.50		13,660.54	9,762.01	10,649.87	920.73	1.13	0.52		1.65
70N 34A26B		0.40	0.34	43.96	2.87	263.52	1,375.27	62.78	24,361.58	71.54	4.50	7.72	74.66	144.99	56,583.15		3.58
80N 16	676.27	10.31	11.40	5.30	119.35	37.39	31,994.57	3,504.68	19,423.33	1,245.36	16,674.15	1,903.43	78.28	1.65	9.41	449.57	62.88
80N 24	161.06		133.92	2.35	1,540.12	1,185.31	3,312.24	1,230.91	1,008.57	394.17	1,739.02	41.33	108.54	205.98	31.86	3,737.45	157.01
80N 31	103.96		0.88	2.94	0.52	1,147.92	175.49	2,272.06	789.93	2,677.43	1,612.85	227.34	20.82	80,047.40	14.12	4.94	257.84
80N 44	64.93	1.49	10.53	2.94	44.04	216.84	36,350.27	104.68	4,374.14	419.19	8,360.31	3.31	17.21	3.63	5.79	121.14	20.46
80N 51	45.85	8.22		95.92	2.08	10,499.38	10.03	5,974.20	7.49	989.70	86.09	659.28	7.22	56,004.93	0.72	10.77	60.28
80N 54	44.31	0.15	0.29		1.30	217.19	6.13	105.43	0.88	34.78	83.81	69.44	11.66	51.82	279.51	8.08	795.86
80N 55	39.71	68.45	0.58	18,962.06	603.02	19,890.72	191.36	5,274.69	1,124.06	4,932.00	2,107.50	1,224.31	28.04	146,287.92	42.00	858.76	421.18
80N 63	30.85	3.59	0.29	1,980.24	338.25	2,927.85	520.61	5,389.80	1.32	308.75	35.53	56.21	0.56	28.06	0.36	996.50	24.56
80N 66	29.48	392.63	18.42	37.66	160,595.58	430.12	80,794.93	7,124.77	70.09	48,649.45	15,007.10	29,879.09	12,917.91	2,527.87	259,962.93	121,131.37	226,706.20
80N 115	11.59	154.24		26,121.53	8.08	789.73	2.79	3,041.10		508.27	35.53	12,717.64	7.50	2,722.95	0.36	38.14	25.67
80N 142	8.35	237.94	0.29	1.18	2.61	815.01	474.37	1.71	1,668.02	982.98	2,433.62	15.29	6.66	3.63	5.07	7.18	58.41
80N 148	7.67	8.82	1.17	14.12	144.89	5,592.93	14,843.39	6,116.10	7,163.13	1,784.75	6,909.61	294.30	14.16	2.97	0.72	476.04	32.74
80N 218	4.60	12.26	19.88	193,564.60	63,235.56	20,200.84	69,134.25	19,385.46	16,780.25	123,856.54	36,850.48	135,422.10	198,429.83	114.87	66,173.59	20,986.23	77,493.57
80N 433	1.53				0.26	24.21	21.73	61.55	0.44	408.81	0.91	398.87	4.44		0.36	1.79	2.60
80N 653	1.02			0.59	1.56	8.90	47.63	233.08	4.41	425.90	44.64	247.18	1,595.38	0.33	10.86	4.04	64.00
80N 938	0.68				0.26	0.36	0.56	0.28	0.44		66.50		0.56	0.66	38.74	0.90	244.45
80N 1632	0.34					9.26	7.24	4.56	2.20		8.20	85.15		45.88			3.77
80N 42A						4.27	1,951.52	411.73	0.44	44.54	2.28	129.38	4.72	18.49		1.35	1.86
80N 46A29B	0.17		0.29			1.78	1,439.55	3.13	0.88	154.37	12.75	76.05	173.22	3.63	1.09	1.35	8.93

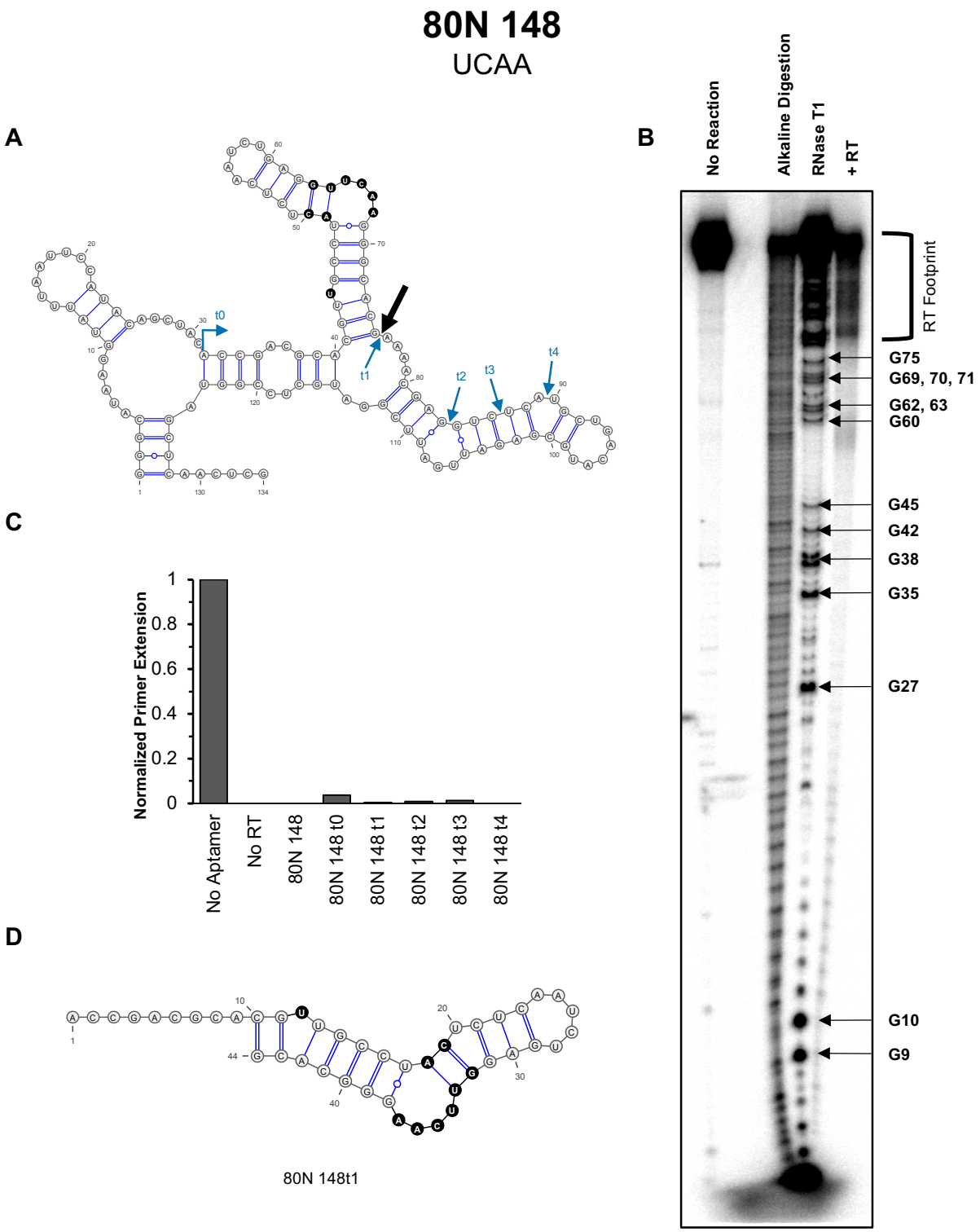

Figure S11 Minimization and motif characterization of 80N 148.

(**A**) The predicted secondary structure of the aptamer with arrows depicting the location of the 3' boundary using RNase T1 digestion (large black arrow), and 3' end truncations that either remain functional (blue) or abrogate inhibition (red). (**B**) RT:aptamer 3' boundary. (**C**) Inhibition of HXB2 RT's DNA-dependent DNA polymerase activity by aptamer truncations. (**D**) The minimally viable 3' end truncation of the aptamer, 80N 148t1.

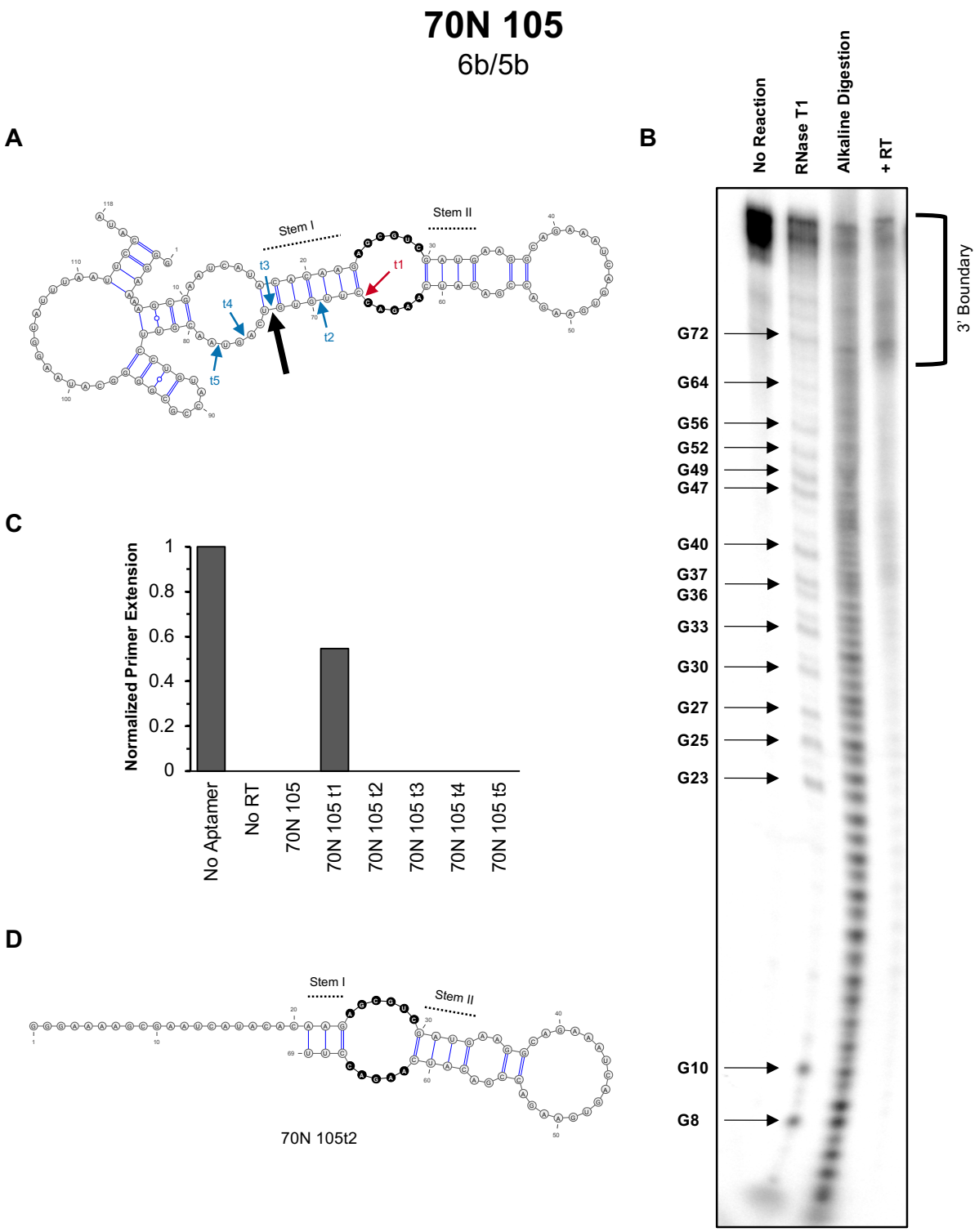

Figure S12 Minimization and motif characterization of 70N 105.

(**A**) The predicted secondary structure of the aptamer with arrows depicting the location of the 3' boundary using RNase T1 digestion (large black arrow), and 3' end truncations that either remain functional (blue) or abrogate inhibition (red). (**B**) RT:aptamer 3' boundary. (**C**) Inhibition of HXB2 RT's DNA-dependent DNA polymerase activity by aptamer truncations. (**D**) The minimally viable 3' end truncation of the aptamer, 70N 105t2.

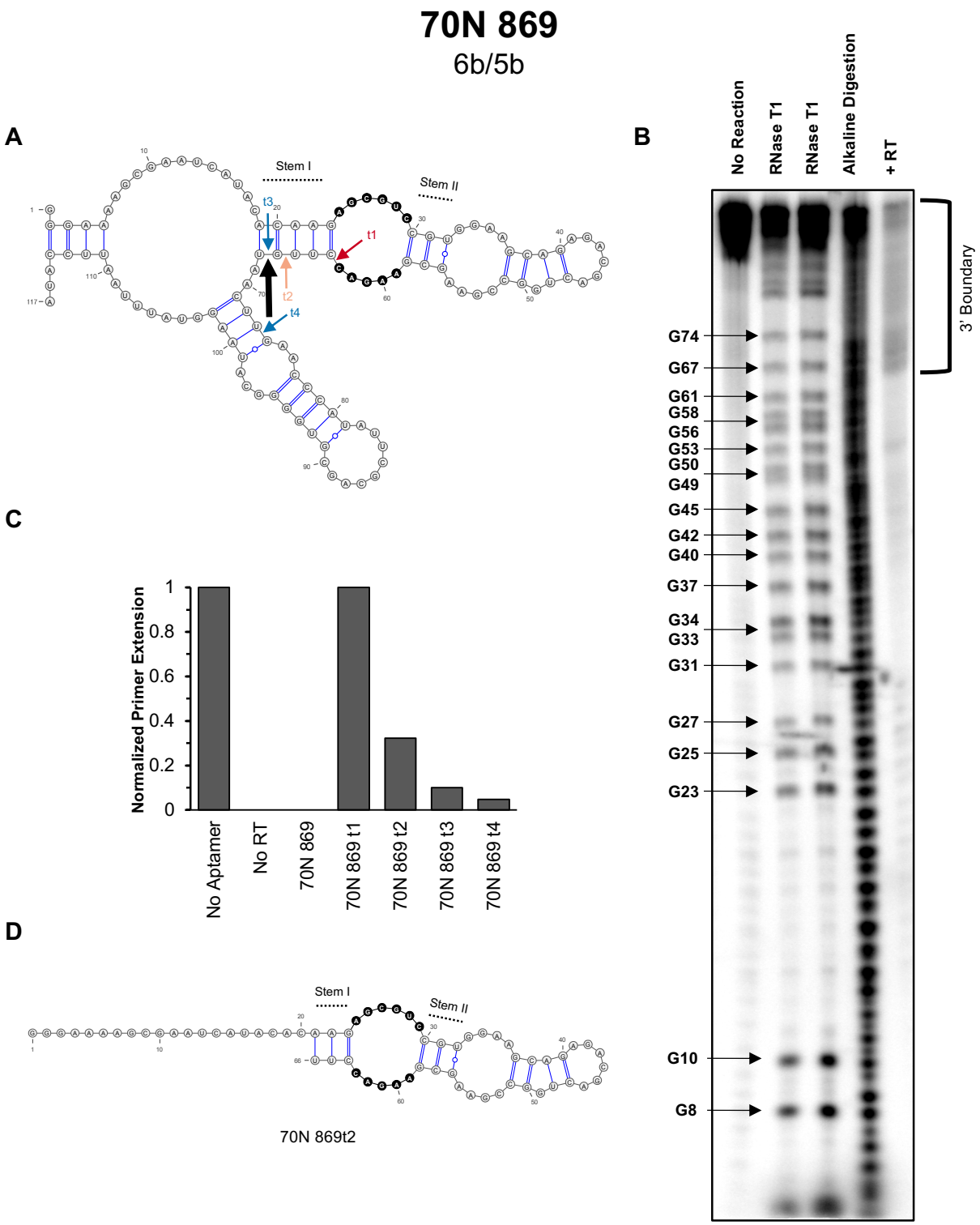

Figure S13 Minimization and motif characterization of 70N 869.

(**A**) The predicted secondary structure of the aptamer with arrows depicting the location of the 3' boundary using RNase T1 digestion (large black arrow), and 3' end truncations that either remain functional (blue) or abrogate inhibition (red). (**B**) RT:aptamer 3' boundary. (**C**) Inhibition of HXB2 RT's DNA-dependent DNA polymerase activity by aptamer truncations. (**D**) The minimally viable 3' end truncation of the aptamer, 70N 869t2.

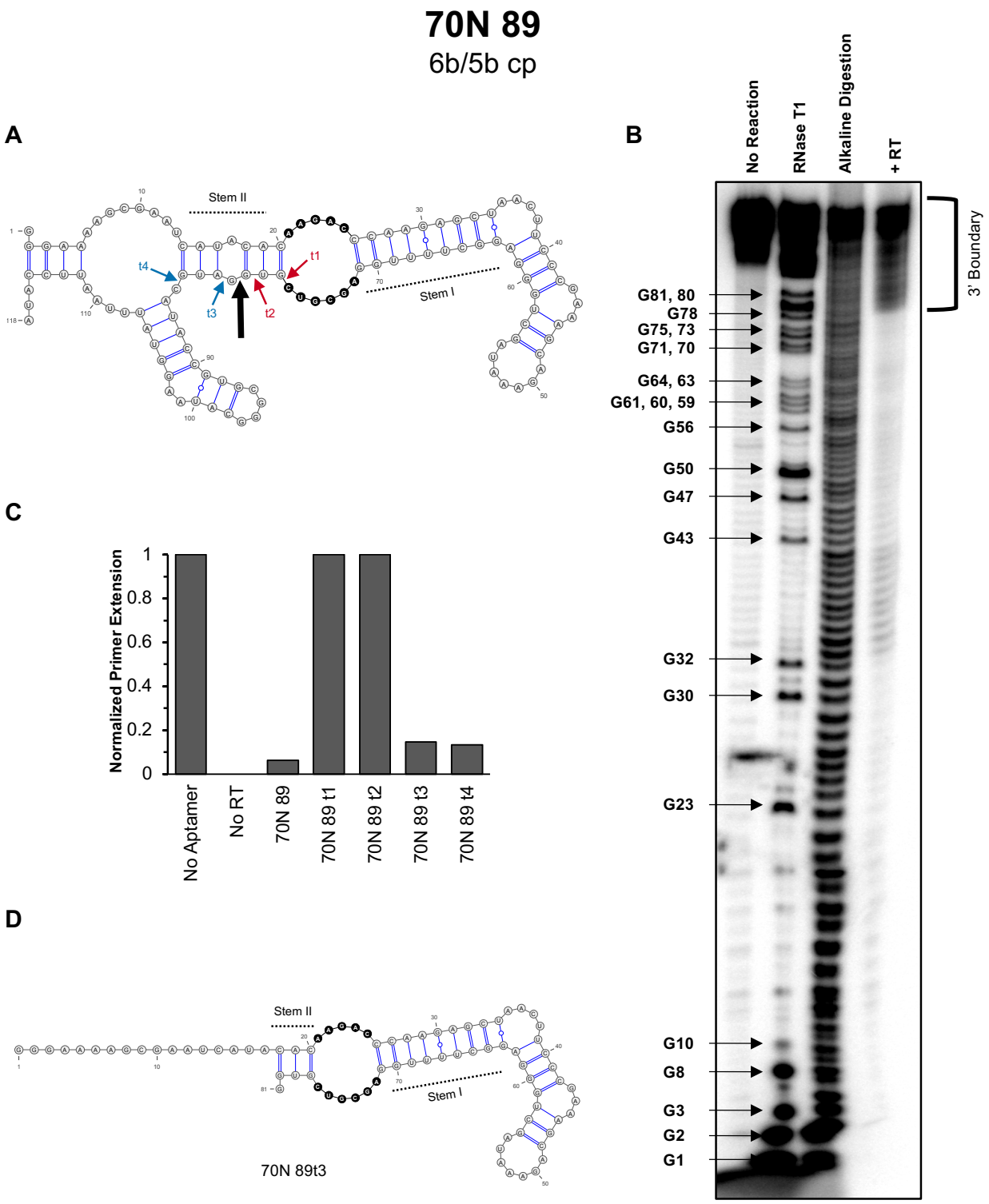

Figure S14 Minimization and motif characterization of 70N 89.

(**A**) The predicted secondary structure of the aptamer with arrows depicting the location of the 3' boundary using RNase T1 digestion (large black arrow), and 3' end truncations that either remain functional (blue) or abrogate inhibition (red). (**B**) RT:aptamer 3' boundary. (**C**) Inhibition of HXB2 RT's DNA-dependent DNA polymerase activity by aptamer truncations. (**D**) The minimally viable 3' end truncation of the aptamer, 70N 89t3.

80N 433

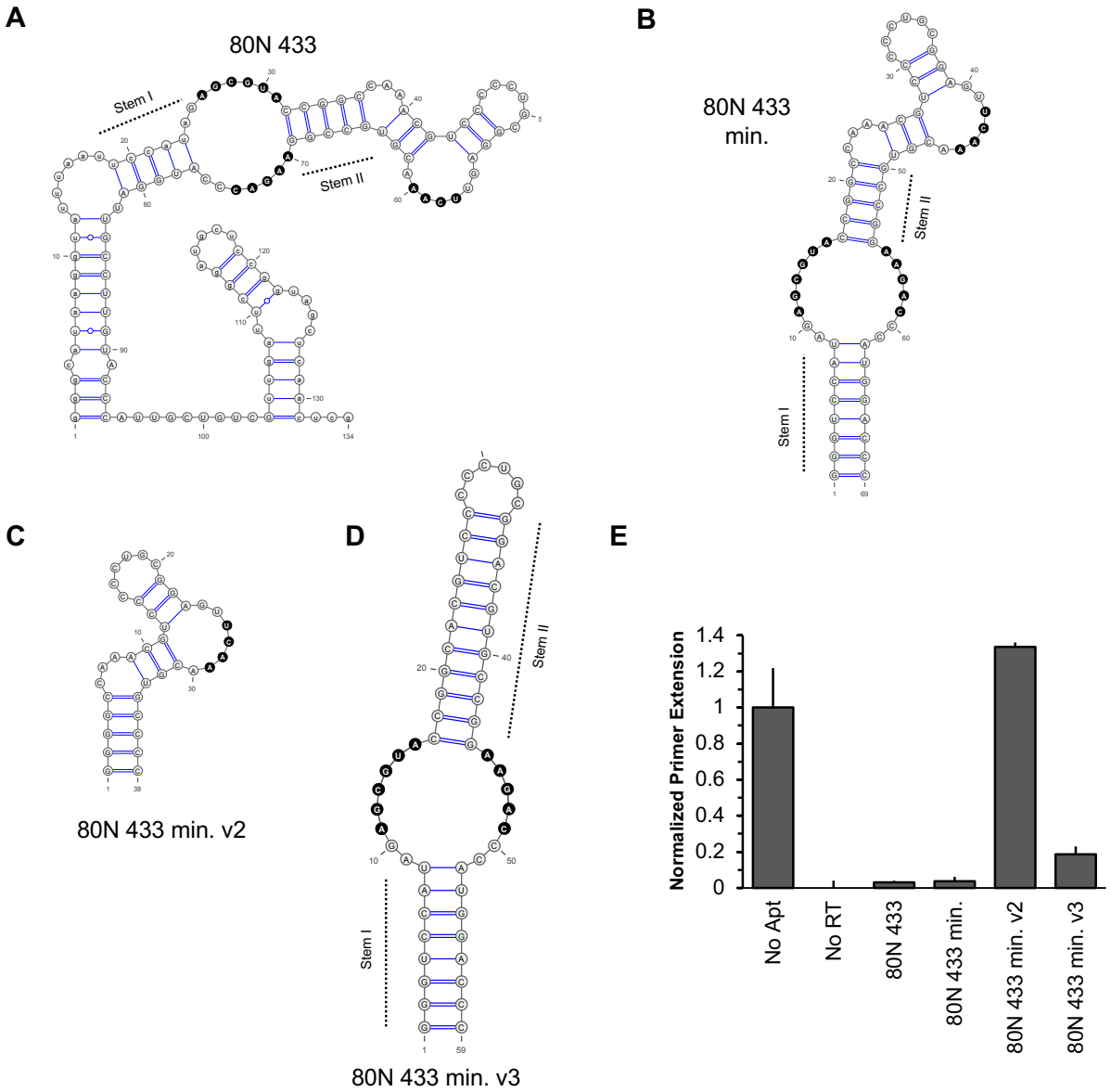

Figure S15 Minimization and motif characterization of 80N 433.

(**A**) The predicted secondary structure of full-length aptamer 80N 433 potentially contains both (6/5)AL and UCAA bulge motifs. Note that Stem I can be extended by two more base pairs if A24 and C76 are tolerated in the penultimate closing position to generate asymmetric loops of the expected 6/5 size. (**B**) 80N 433 min., a minimized variant of 80N 433, contains a 5' GGG to increase transcriptional yield using T7 RNA polymerase and a corresponding 3' CCC to base pair. (**C**) 80N 433 min. v2 is a variant of the minimal aptamer in which the (6/5)AL motif has been removed, leaving only the bulges. (**D**) 80N 433 min. v3 is a variant of the minimal aptamer in which the predicted CAA and UCAA bulges have been removed, leaving only the (6/5)AL motif. (**E**) Primer extension assays against HXB2 RT. The minimal aptamer, 80N 433 min., shows similar inhibition to the full-length aptamer. Deletion of the (6/5)AL motif in 80N 433 min. v2 abrogates the inhibitory function of the aptamer. Removal of only the bulges (including the UCAA-containing bulge) reduces the primer extension ability of HXB2 RT but remains less inhibitory than the variants containing both the bulges and the (6/5)AL motif.

80N 44

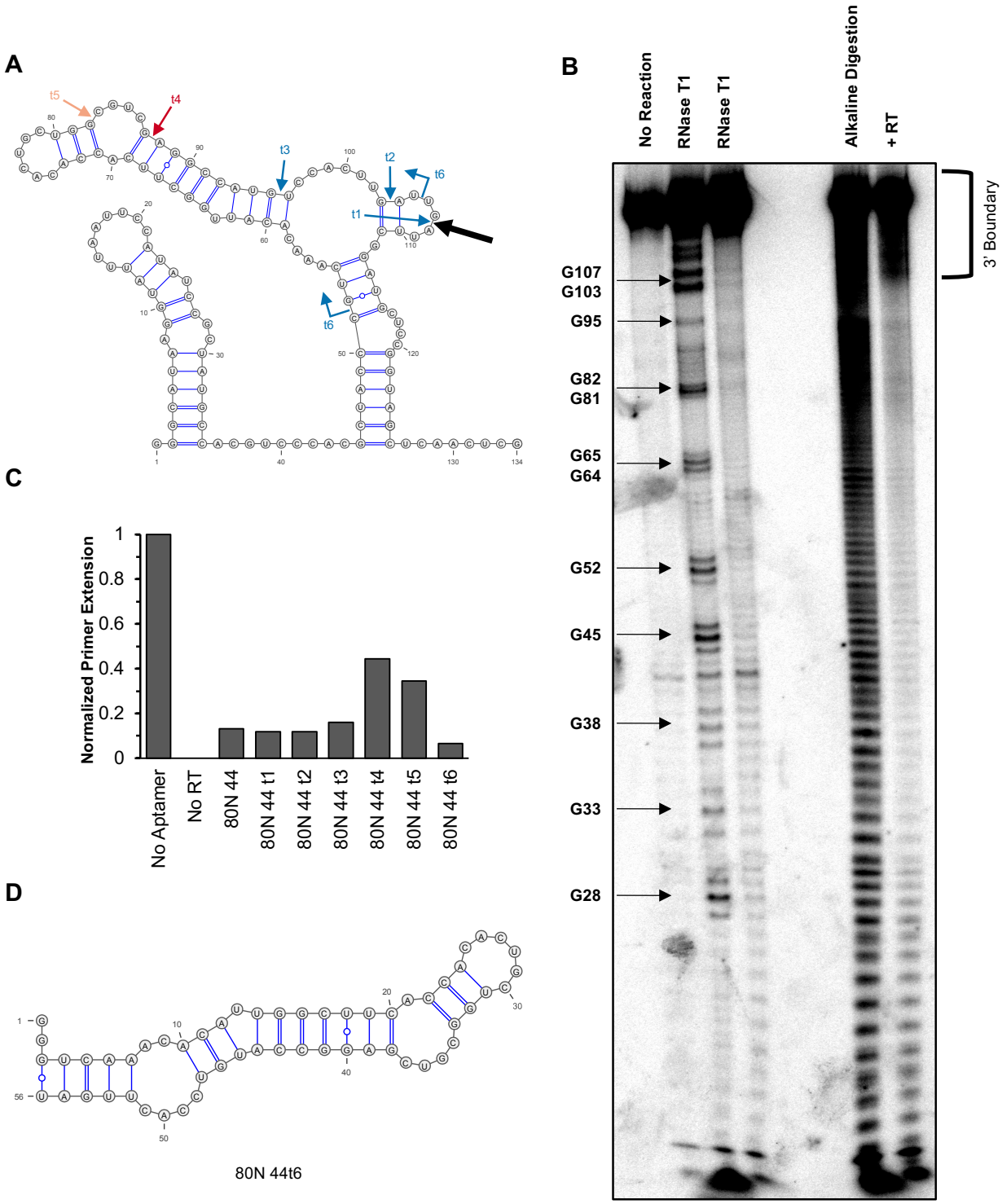

Figure S16 Minimization and motif characterization of 80N 44.

(**A**) The predicted secondary structure of the aptamer with arrows depicting the location of the RT footprint using RNase T1 digestion (large black arrow), and 3' end truncations that either remain functional (blue) or lower inhibition (orange/red). Truncation 6 (t6) is truncated from both 5' and 3' ends. (**B**) RT:aptamer 3' boundary. (**C**) Inhibition of HXB2 RT's DNA-dependent DNA polymerase activity by aptamer truncations. (**D**) The minimally viable 3' end truncation of the aptamer, 80N 44t6.

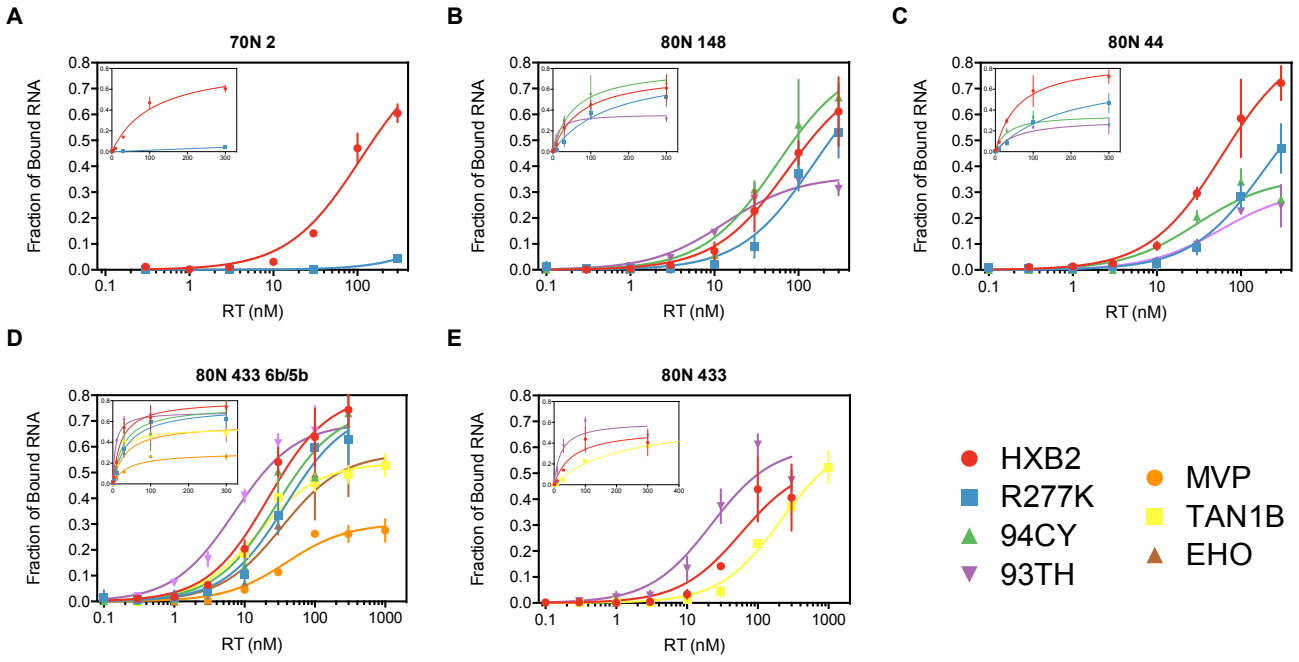

Figure S17 Binding curves for candidate aptamers against various RTs.

Trace amounts of 5' radiolabeled aptamers were incubated with varying concentrations of the indicated RTs. Retention of radiolabel after nitrocellulose filtration was measured and data were fit to a one site binding curve using Prism GraphPad 6.2. Data shown are from triplicate experiments with error bars to indicate standard deviation. Insets show the same data plotted with a linear *x*-axis.

Table S6 – Aptamer sequences used in this study[a]

70N 2 (F1Pk)
gggaaaagcgaaucauacacaagaCAUAGCGACUGUCCACGAA**UCCG**AAGCCUAA**CGGGACAA**AAGGCAAGAGCGCGAUACCAAUGCUGGACUGgggcaua
agguauuuaauuccaua

70N 3 (F1Pk)
gggaaaagcgaaucauacacaagaAACCGCAAGCAACACCCAGCAAGAAACA**UCCG**ACGCACGA**CGGGAGAA**AGUGCAUUACCACGAUGUCGAUgggcaua
agguauuuaauuccaua

70N 8 (6a/5a)
gggaaaagcgaaucauacacaaga**ACGUU**GUGCACGGAUGCCCACGGUCGCAC**GAAAC**CUUGUGUGGGAUAGCGCGAAUACUGACGAGUGUGCCgggca
uaagguauuuaauuccaua

70N 11
gggaaaagcgaaucauacacaagaACCAAGAUAAACCGAGGUGUAAACGGGAAAACACAUGGAAUGACGUGCUGUAGUAGGUGUGAUCACUGCgggcauaa
gguauuuaauuccaua

70N 27 (F1Pk)
gggaaaagcgaaucauacacaagaUGGCAAGUACCUUGGA**UCCG**AAGAAAA**CGGGAAAA**UUGACAAAGUGAAAGGAAUUACCGUACCGAGGGUGgggcaua
agguauuuaauuccaua

70N 36 (F1Pk)
gggaaaagcgaaucauacacaagaCCCGCACCAAAUGAAGA**UCCG**AGACCAA**CGGGAAAA**UGGUCACACCAAGGAAUAGAUGCACGCCUCACAUgggcaua
agguauuuaauuccaua

70N 50 (F1Pk)
gggaaaagcgaaucauacacaagaGAGAAUGCUGAUCCAAGUGA**UCCG**AACUACAA**CGGGAGAA**CGUAGAACCACACGAUACACCACAGCGgggcauaaggu
auuuaauuccaua

70N 55
gggaaaagcgaaucauacacaagaCCUAGGUGAUAAAAGGGAUAACACAAGCGAGAAUACAUUGAACAUGCCAUGUGCGACGUAACCCAGCGGAgggcaua
agguauuuaauuccaua

70N 73 (F1Pk)
gggaaaagcgaaucauacacaagaA**UCCG**AAGGAACA**CGGGAGAA**ACCAAUACUGGAAGAUUAUCCAAUUGCCACGGACAAGCAUCCCACGGAAgggcaua
agguauuuaauuccaua

70N 89 (6b/5b cp)
gggaaaagcgaaucauacac**aaga**C**C**CCAAGAGCUAACUUCCCGAAAGCAGAAAUAGCUGGGAGGCUUUUGG**AGCGUC**GUGGAUGCAUACCGUGCgggcau
aagguauuuaauuccaua

70N 105 (6b/5b)
gggaaaagcgaaucauacacaaga**GCGUC**GAUGAAGGCAGAAAUCAGUGAAGACCGACAUC**AAGAC**CUUGUGUCAGUAACGUUCCUGUACCGCGgggcau
aagguauuuaauuccaua

70N 144 (F1Pk)
gggaaaagcgaaucauacacaagaCCGCACGAAGAAA**UCCG**AGGUGAUAAA**CGGGAGAA**CACAAACCGCUCUAAUUGAAGGCACCCGCACGCGAgggcaua
agguauuuaauuccaua

70N 177 (6a/5a)
gggaaaagcgaaucauacacaagaG**AACGUU**GGUGAGCCUCAUAGGGAGCAAUGAGGACGACC**GAAAC**CUCUCGUGUAAGCUGGUCCGUGACUGgggca
uaagguauuuaauuccaua

70N 869 (6b/5b)
gggaaaagcgaaucauacacaaga**GCGUC**CGUGGAAGCAGAGACGACUGGCCGAAGCG**AAGAC**CUUGUAACUUGAACCCAUAUUCGCAGCGUGgggcaua
agguauuuaauuccaua

70N 24A28B (6d/5a)
gggaaaagcgaaucauacacaaga**ACGUG**CUAGACACGCAUCAGAACGAUGAAAGGUGACUAG**GAAAC**CUUGUGGAUUACGCGCGUUGAUCGUUgggcau
aagguauuuaauuccaua

70N 34A26B
gggaaaagcgaaucauacacaagaGCGACGGCUUGAGUGAAGACGAAUCAGCAGACCAAAAAAUACCGAGUGAAGAGGAAGGGUAACGAGGAGgggcauaa
gguauuuaauuccaua

88.1 (6b/5b cp)
gggaaaagcgaaucauacac**aaga**C**C**AUUGACCAAAAGGGUCGAU**AGCGUC**GUGUAGAUUGCACCCAUGACUGAGCUACUGCCAAAUCCACCCACgggcaua
agguauuuaauuccaua

88.1 6c/5b (6c/5b cp)
gggaaaagcgaaucauacac**aaga**C**C**AUUGACCAAAAGGGUCGAU**AACGUC**GUGUAGAUUGCACCCAUGACUGAGCUACUGCCAAAUCCACCCACgggcaua
agguauuuaauuccaua

88.1 6f/5b (6f/5b cp)
gggaaaagcgaaucauacac**aaga**C**A**UUGACCAAAAGGGUCGAU**AGCGUA**GUGUAGAUUGCACCCAUGACUGAGCUACUGCCAAAUCCACCCAC gggcaua agguauuuaauuccaua

A9 (6b/5b cp)
gggaaaagcgaaucauacac**aaga**C**U**CCACAAGAAAGGAAGGUGGA**AGCGUC**GUGUGUGAAAGCAAGUAAGAAGAUGUGCAUGCCUGCCGCGAU gggcau aagguauuuaauuccaua

x1.1 (6a/5a)
gggaaaagcgaaucauacacaaga**aACGUU**GUCGAAAGCCUAUGCAAAUUAAGGACUGUCGAC**GAAAC**CUUGCGUAGACUCGCCACGCUUGGUGU gggcau aagguauuuaauuccaua

80N 16 (UCAA)
gggcauaagguauuuaauuccauaGCAACCGGUUGUCUACACGCGGCGAAUAGAGCCCGGU**UCAA**GGACACCGCCACUGCUGUCGACAUUUCCUUAGU GCUAGAuugauucggaugcuccgguagcucaacucg

80N 24 (F1Pk)
gggcauaagguauuuaauuccauaUCCUCACCCAAAUUGA**UCCG**ACGCACGA**CGGGACAA**UGUGCAACCCUGCUACCACACCGUUCUCGGACUACCCCC CUCAGuugauucggaugcuccgguagcucaacucg

80N 31
gggcauaagguauuuaauuccauaGUCCAACACUCCCGUCGCCGAAACCCUUGCCAUAAACAAUCCUGACCGAUGGAUCAGGGAGAAAUCGUCCAUCAG ACAUUuugauucggaugcuccgguagcucaacucg

80N 44
gggcauaagguauuuaauuccauaUCCGCUAUGCCACGUCCCACGCUACCCGUCAAACACAUUGGCUUCACCACACUGCUGGCGUCGAGGCCAUGUCCA CUUGAuugauucggaugcuccgguagcucaacucg

80N 51 (6g/5a)
gggcauaagguauuuaauuccau**aGCCUC**ACCAAUCCUCGU**GAAAC**GGAGGGAUAAACGUUUUCAGAAGAUGUCACACUCAUUACGCCUGACCUUGAUU UGACUuugauucggaugcuccgguagcucaacucg

80N 54
gggcauaagguauuuaauuccauaCCUCCCUCGAACGGAACACAAUUUGGGUCAACUUGUCCCGAUGCAGGGGUGGGUGGUGUGGUUAUGCGUCGUGU ACAAGAuugauucggaugcuccgguagcucaacucg

80N 55 (F1Pk)
gggcauaagguauuuaauuccauaUCGCUCCACAACUAACGA**UCCG**AAGACCA**CGGGAUAA**GGUCACUCCUUUCAGAAGCAUACUACAUUCGGCACCGA AUUGAuugauucggaugcuccgguagcucaacucg

80N 63
gggcauaagguauuuaauuccauaCGUGACCCUGAAUCCCAGGUGUAAAGGGGAUAACACAACUUUUGGUUCCGCCAAUGCUGAGUGGCGCAUUCCAUG AUCUGuugauucggaugcuccgguagcucaacucg

80N 66
gggcauaagguauuuaauuccauaUCCGUCACCAUGCAACACCAGACACUCUGUACCAAUGGGUCAGGGACUGAGGGAAUGGGUGGUACUUGUCACGU GUGUUGuugauucggaugcuccgguagcucaacucg

80N 115 (F1Pk)
gggcauaagguauuuaauuccauaCCUCAACCACACGAUGAA**UCCG**AAGAGUAA**CGGGAUAA**UACUCGAAUACGCGUAUACAGUUGAGUGACGCUUUCA UCUGUuugauucggaugcuccgguagcucaacucg

80N 142 (UCAA)
gggcauaagguauuuaauuccauaCGGUACGUGGACGCGUUGCAAACUCGAUUAGGAAAGU**UCAA**CUGCACGCUAUCCAAUACCUACGGCACCAUAUUC GAUUGuugauucggaugcuccgguagcucaacucg

80N 148 (UCAA)
gggcauaagguauuuaauuccauaCAGCUACACCGACGCACGUUGCCUACUCUCAAUCUGAGGU**UCAA**GGGCACGAAAACGAGGUCUCAUGCUGACAUG CGAGAuugauucggaugcuccgguagcucaacucg

80N 218 (6a/5a)
gggcauaagguauuuaauuccauaUCGCACCACUGG**AACGUU**GCACAGGACAGUAUCGGUUUGUGUUCAGUGC**GAAAC**CCAGAGUGGAUGUACUUUGU UGAUUCuugauucggaugcuccgguagcucaacucg

80N 433 (6f/5b & UCAA)
gggcauaagguauuuaauuccauaG**AGCGUA**CCGGCCAAACGUCCCCCUGCGGAGU**UCAA**ACGUGCCGG**AAGAC**CCAUGGAUUGCCUUGUACCCAUUG CUGUCGuugauucggaugcuccgguagcucaacucg

80N 433 min. (6f/5b & UCAA)
GGGUCCAUAG**AGCGUA**CCGGCCAAACGUCCCCCUGCGGAGU**UCAA**ACGUGCCGG**AAGAC**CCAUGGACCC

80N 433min2 (UCAA)
GGGGCCAAACGUCCCCCUGCGGAGU**UCAA**ACGUGCCCC

80N 433min3 (6f/5b)
GGGUCCAUAG**AGCGUA**CCGGCACGUCCCCCUGCGGACGUGCCGG**AAGAC**CCAUGGACCC

80N 653 (6b/5b cp)
gggcauaagguauuuaauuccauaGGUGAC**AAGAC**CAGCCAAACAUCUGGACACAACUCCACAUGUCGGCUG**AGCGUC**GUCAUCUAAUGCGUGACGAGA
AUGAGuugauucggaugcuccgguagcucaacucg

80N 938
gggcauaagguauuuaauuccauaGACCGAUCCAACUGCUGGGACUUGCGAAAGGGGAAAGGGAAUGGGAAGGGACGCAACUCCUGUUCAUGUUGAUU
CGGAUGuugauucggaugcuccgguagcucaacucg

80N 1632
gggcauaagguauuuaauuccauaCACGACAAACAGGCUAUUCUUGGCAAGGGCCUGGAGUAUUCCCUACUUCGAAAGAUGAGUCUUAUAACCUUGCGC
CACGAuugauucggaugcuccgguagcucaacucg

80N 42A (6c/5b cp)
gggcauaagguauuuaauuccauaACCGAAUACUCGCGC**AAGAC**CCCUUUCUCUCGAGACUGUGG**AACGUC**GCACGAGUGAUACCCACGACCGCUUUU
CCUUGCuugauucggaugcuccgguagcucaacucg

80N 42A 6b/5b (6b/5b cp)
gggcauaagguauuuaauuccauaACCGAAUACUCGCGC**AAGAC**CCCUUUCUCUCGAGACUGUGG**AGCGUC**GCACGAGUGAUACCCACGACCGCUUUU
CCUUGCuugauucggaugcuccgguagcucaacucg

80N 46A29B (6a/5d)
gggcauaagguauuuaauuccauaCUCGCUCGUUGG**AACGUU**GUUUGAUGGCCAUCCAGGAAUUGGCCGAUCAAGC**UAAAC**CCAGCGAUAGUUGCUCA
UUGUCUuugauucggaugcuccgguagcucaacucg

[a]Constant regions are shown in gray. Identified motifs are shown in bold with flanking stems underlined.